NATIONAL ADVISORY COMMITTEE FOR AERONAUTICS

TECHNICAL NOTE 3885

INVESTIGATION OF TRANSIENT POOL BOILING DUE TO SUDDEN LARGE POWER SURGE

By Robert Cole

Lewis Flight Propulsion Laboratory
Cleveland, Ohio

Washington
December 1956

NATIONAL ADVISORY COMMITTEE FOR AERONAUTICS

TECHNICAL NOTE 3885

INVESTIGATION OF TRANSIENT POOL BOILING DUE TO SUDDEN LARGE POWER SURGE

By Robert Cole

SUMMARY

The transfer of heat from a metallic ribbon to water, under transient conditions, was studied for initial water temperatures from 76° to 203° F and average heat-generation rates per square foot of surface area of 3, 10, and 20×10^5 Btu per hour per square foot. The tests were conducted at atmospheric pressure under pool boiling conditions. The power surge duration was held constant at 30 milliseconds.

An analysis assuming time periods of such short duration that free-convection effects are negligible was successful in predicting ribbon temperatures as a function of time and heat-generation rate in the nonboiling region. A simplified analysis assuming the ribbon to be completely insulated was found to be applicable during time periods in the nonboiling region of short duration. In addition, the analysis was found to be applicable for the entire surge duration under conditions of heat-generation rates well above those required for film boiling.

Transient critical heat flux values up to 3×10^6 Btu per hour per square foot were obtained for water at atmospheric pressure. The obtained data indicated an increase in critical heat flux with increase in the degree of subcooling for a constant heat-generation rate, and an increase in critical heat flux with increase in the rate of heat generation for a constant degree of subcooling.

INTRODUCTION

Of current interest in the field of nuclear reactor design is the problem of fuel element burnout due to a sudden large power surge. In the advent of an exponential power surge resulting from a step change in reactivity, where a subcooled liquid is used as a coolant, the wall temperature rises rapidly until it has exceeded the saturation temperature of the fluid. As a consequence of the temperature excess, surface

(nucleate) boiling occurs resulting in an increase in the rate of heat transfer. Provided that the heat-generation rate is still greater than the rate at which heat is being transferred, vapor formation increases until a point is reached at which the bubbles coalesce (film boiling). The increased thermal resistance, due to the film of vapor, causes a rapid decrease in the heat-transfer rate and a corresponding rise in wall temperature, resulting in the eventual melting of the fuel element.

To determine the minimum safe reactor period (the minimum time taken for the power to increase by a factor of e without endangering the reactor) which is allowable with a given control system design, a knowledge of the heat-transfer characteristics during the surge duration is required (ref. 1). The purpose of this paper is to give an insight into the transient heat-transfer characteristics of a liquid-cooled system during a sudden power surge. The experimental system consisted of an electrically heated nickel ribbon immersed horizontally in a pool of water, with a sudden large power surge created by a step change in voltage.

APPARATUS AND PROCEDURE

Main Circuit

The main circuit (fig. 1) contained a nickel ribbon suspended horizontally by means of two copper rods in a pool of boiled distilled water, a calibrated resistance, and a bank of four 12-volt storage batteries. The nickel ribbon, which was 3 inches by 0.15 inch by 0.005 inch, was heated electrically by a current pulse originating in the storage batteries. The two copper rods acted as heat sinks and remained at the same temperature as the mass of water in which the ribbon was submerged. By means of a dual-channel oscillograph and an oscillograph-record camera, the voltage drop across the copper rods, which was essentially that across the ribbon, and the voltage drop across the shunt were measured and recorded as a function of time. Instantaneous values of average temperature and heat-generation rate were obtained from these measurements since the ribbons had previously been calibrated as resistance thermometers. Variations in liquid subcooling and heat-generation rate were accomplished as follows. For a given series of runs, the voltage drop across the ribbon was held constant and the degree of subcooling varied. The voltage drop was then increased and held constant while the degree of subcooling was again varied. This procedure was followed until a voltage drop setting was reached at which the ribbon failed. For a given voltage drop setting, the initial heat-generation rate decreased by a maximum of 13 percent as the degree of subcooling decreased. Also for a given run, the heat-generation rate decreased by as much as 50 percent with time. In order to distinguish between the various levels corresponding to a given voltage drop, an average value for each is used throughout the report.

Timing Circuit

The timing circuit (fig. 2) regulated the following items by means of a group of relays and a motor-driven bank of timing wheels: a 16-millimeter camera, a flash bulb, the driven sweep of the oscillograph, and the power surge duration. The camera, operating at a rate of 5000 frames per second, recorded the boiling action on the ribbon. The individual frames on the film were related to the voltage traces on the oscillograph by means of 1000-cycle-per-second timing marks applied simultaneously to the z-axis of the oscillograph and an argon timing lamp within the camera.

Methods of Calculation

The basic data needed for the determination of the system heat-transfer characteristics are the simultaneous voltage drops across the ribbon and a calibrated resistance in series with it. The voltage drops were determined as a function of time by means of a dual-channel oscillograph and an oscillograph-record camera. Calibration was obtained on each print by means of a known square wave voltage for each beam, obtainable from the oscillograph.

Rate of heat generation. - The instantaneous rate of heat generation was determined by the product of the voltage drop across the ribbon and the line current which is obtainable from the voltage drop across the calibrated resistance

$$P = 3.413\ vI \tag{1}$$

Symbols are defined in appendix A.

Average ribbon temperature. - The ribbon resistance was determined from voltage and current measurements by the assumption of a pure resistance circuit

$$R(\theta_w) = \frac{V}{I}$$

Calibration of the nickel ribbon as a resistance thermometer determines the instantaneous average ribbon temperature. The calibration curves of resistance as a function of temperature are given in figure 3.

Rate of heat transfer. - The rate of heat generation is given by equation (1). The rate of heat absorption is given by

$$wc_p \frac{d\theta_w}{dt}$$

Neglecting end losses, the difference between these two quantities must equal the instantaneous average heat flux

$$q = \frac{1}{S}\left(3.413\ vI - wc_p \frac{d\theta_w}{dt}\right) \tag{2}$$

with $d\theta_w/dt$ obtained from a plot of average ribbon temperature against time. The c_p term was obtained as a function of average ribbon temperature by the relations (ref. 2)

$$c_p = 4.26 + 0.00640\ T \quad (T = 273^\circ \text{ to } 626^\circ\ K)$$
$$c_p = 5.99 + 0.000905\ T \quad (T = 626^\circ \text{ to } 1725^\circ\ K)$$

(cal/(deg)(mole)

To justify the neglect of end losses in equation (2), an analytical expression is developed in appendix B to illustrate the type of temperature distribution obtainable along an internally heated slab of finite length, each end of which is in contact with a heat sink, if the mode of heat transfer is assumed to be solely by conduction along the length of the slab. The length of the slab was taken to be 3 inches, and a heat-generation rate comparable to those resulting experimentally was used. From the results shown in figure 4, the heat loss through the ribbon terminals was calculated to be 0.26, 0.28, and 0.3 percent at 2, 5, and 8 milliseconds, respectively.

Heat-transfer coefficient. - The heat-transfer coefficient, based on average ribbon temperature rather than surface temperature, is defined by the equation

$$q = h(\theta_w - \theta_o)$$

The instantaneous average heat-transfer coefficient was therefore determined by the value of q previously obtained and the corresponding temperature difference.

RESULTS AND DISCUSSION

Because of the very short time periods employed, it might be expected that average ribbon temperatures could be predicted with a fair degree of accuracy in the initial moments of the period by assuming the ribbon to be completely insulated. Figure 5 illustrates the divergence of the experimental data from that assumption. The maximum deviation of the average ribbon temperature in the nonboiling region was 43 percent. In the nucleate boiling region, as the initial system temperature was

increased, the deviation from the assumption of complete insulation increased. In the partial and complete film boiling regions, the deviation decreased with increasing initial system temperature, approaching a value of constant magnitude. In appendix C, an analytical expression for the average ribbon temperature is developed assuming the ribbon to be completely insulated.

Because of the fair agreement found in the nonboiling region, the possibility arises that during the short time period used free-convection effects are negligible and, therefore, that heat transfer to the surrounding medium is by the process of conduction. In appendix B, it is shown that heat loss through the ribbon terminals was negligible. Since the ratio of ribbon width to ribbon thickness was 30, it may be assumed that the major portion of the heat flow was through the face of the ribbon. Thus, the problem may be considered one-dimensional. In appendix D, analytical expressions are derived for the temperature distribution through the ribbon thickness and into an infinite medium. The resulting distribution, using the same heat-generation rate as in figure 4, is given in figure 6. Although it may be seen from figure 6 that the temperature distribution within the ribbon was quite flat, for completeness, an analytical expression is derived in appendix E for the average ribbon temperature.

In figure 7, the average ribbon temperatures as derived in appendixes C and E are compared with the experimental data. The agreement with appendix E is excellent, bearing out the validity of the assumption. Such agreement also indicates that in the nonboiling region, the average temperature of the ribbon did not deviate greatly from its surface temperature. Thus, in the nonboiling region, heat-transfer coefficients would correspond to those based on surface temperature measurements. In the nucleate boiling region, there is some uncertainty as to the deviation of surface temperatures from average temperatures. However, since the average temperatures measured seem to correspond in magnitude to surface temperatures normally encountered in nucleate boiling, the calculated heat-transfer coefficients should be at least usable. Figures 8 and 9 are typical records of the variation of heat flux and heat-transfer coefficient with time and average temperature difference, corresponding to the temperature-time curves in figure 7.

Nucleate Boiling Region

Average ribbon temperature. - No reliable prediction of the ribbon temperature could be made in the nucleate boiling region. The ribbon temperatures ranged from 220° to 280° F depending upon the rate of heat generation and degree of subcooling. The average of the ribbon temperatures in the nucleate boiling region was 250° F from which the deviation was ±16 percent.

The transient behavior of the average ribbon temperature in the neighborhood of the inception of boiling is such that the temperature gradient decreased, deviating from the analysis of appendix D. Depending upon the rate of heat generation, degree of subcooling, surface conditions, and gas content, a peak in the temperature curve may result, such that a discontinuity is obtained in the temperature gradient. Figure 10 illustrates this condition. The discontinuity has also been observed in an investigation similar to the present one by using an exponentially increasing heat-generation rate (ref. 3).

Heat transfer. - The inception of nucleation disturbs the thermal boundary layer, and the resultant turbulence causes a sharp increase in the rate of heat transfer. Depending upon the rate of heat generation and the degree of subcooling, the bubbles may expand and collapse, leave the ribbon entirely, or coalesce to form a film of steam completely surrounding the ribbon. Under the first two conditions, the rate of heat transfer approaches some steady-state value.

Excerpts from the film record of the boiling action corresponding to figures 7(c), 8(c), and 9(c) are shown in figure 11. Comparison of the variation in the heat-transfer characteristics with boiling action may be made, as the elapsed time between the initiation of the surge and the exposure of the particular frame is indicated.

By reference to figure 8(c), it may be inferred that surface boiling began at approximately 1.6 milliseconds after the initiation of the power surge, since at this time its effects on the heat-transfer coefficient were noticeable. Thus, the first frame shown in figure 11 was exposed approximately 1 millisecond after the inception of boiling. The bubbles which seem to be in the process of leaving the ribbon were located on the walls of the pyrex beaker and should not be associated with the vapor formation on the ribbon. Figure 7(c) shows that in the time period from 2 to 3 milliseconds, the temperature curve deviated from that predicted in appendix E. Between 2.7 and 3.1 milliseconds, the bubbles grew radially retaining their hemispherical shape. As they grew and as new bubbles formed, more surface area was covered by vapor. Thus, at some point the thermal resistance of the partial vapor film overcame the decrease in thermal resistance resulting from the turbulence caused by the growth of new bubbles and expansion of old bubbles, with the result that at 3 milliseconds the rate of heat transfer began to decrease (fig. 8(c)). From figure 7(c) it may be seen that an inflection occurred at the same instant, and the temperature gradient began to increase. The formation of new bubbles and growth of older ones continued with the result that the bubbles partially coalesced, giving rise to what is known as the partial film boiling region. At 6.7 milliseconds, the ribbon seemed to be surrounded completely by bubbles. However, large individual bubbles in the outer regions were still discernible. At 8.4 milliseconds, the bubbles had coalesced to the extent that a film of vapor surrounded the

ribbon. Figures 7(c), 8(c), and 9(c) show that the rate of heat transfer leveled out and began to increase and the temperature gradient slowly decreased. These characteristics are associated with what is known as the stable film boiling region. The absence of data after a time duration of 18 milliseconds was due to a partial obscuring of the voltage trace at that time plus the fact that the ribbons were not calibrated past 800° F. After 18 milliseconds the heat-generation rate continued to level out, and it may be assumed that the ribbon temperature continued to rise. The actual length of the surge duration was 26 milliseconds. Referring again to figure 11, it should be noticed that there was only a very thin film covering the bottom of the ribbon; thus the expansion of the film occurred on the upper face. At 13.0 milliseconds, there was a noticeable disturbance of the film close to the upper face of the ribbon. This disturbance grew until at 25 milliseconds, the entire film seemed to be tearing away. An interesting feature of the series of frames from 25 to 35.4 milliseconds was the seemingly thin membranelike sheet of film which connected the leaving vapor with the thin film remaining on the ribbon. At 45.3 milliseconds, the vapor bubble had completely dissociated itself, leaving thin films of seemingly equal thickness on the top and bottom of the ribbon.

In general, the first observable density disturbance occurred at the moment at which the ribbon temperature began to deviate from its predicted value. The disturbances (vapor bubbles), when first observed, were hemispherical in shape and had a height of the order of 0.005 inch. The disturbances expanded rapidly and broke up the thermal boundary layer, the resulting increase in heat transfer causing the slope of the temperature-time curve to approach zero.

The subsequent expansion of the bubbles perpendicular to the ribbon was dependent upon the degree of subcooling of the surrounding medium. For low degrees of subcooling, the bubbles retained their hemispherical shape while expanding. As the degree of subcooling increased, the rate of expansion perpendicular to the ribbon decreased and the bubbles tended to grow horizontally along the length of the ribbon. In both instances, many of the individuals combined to form larger bubbles which instead of collapsing completely, as in the case of single disturbances, reacted to present a pulsating type of motion. Although these bubbles did coalesce to some extent, the positions of the individuals were still discernible.

It might be remarked that the growth of many of the disturbances perpendicular to the ribbon was essentially complete at the time they were first observed. Since the film rate was 5000 frames per second, the bubbles had grown to vertical maturity in less than 1/5 of a millisecond.

No correlations were obtained in the nucleate boiling region for either heat-transfer coefficients or rates of heat transfer. In all cases, the inception of boiling was marked by a sharp increase in the heat-transfer coefficient. The behavior of the coefficient under transient conditions is interesting. Although considerable error could have been introduced by the necessity of having to measure temperature gradients, the results in general appear to be quite consistent. As noted previously, h should decrease as the thermal boundary layer builds up. Generally, such was the case. Under these conditions, the coefficient decreased until the boundary layer was disturbed by the formation of small vapor bubbles. The resultant sharp increase in h, caused by the turbulence, gave rise to a minimum condition. In most cases this minimum was so well defined, especially for a plot of h against $\theta_w - \theta_o$, that the corresponding average ribbon temperature and time at which nucleation occurred may be obtained directly, without photographic equipment.

Values of nucleate boiling heat-transfer characteristics obtained in this investigation are tabulated in table I. Only those values which occur prior to the critical heat flux are listed for cases in which film boiling dominates. For cases in which a negative temperature gradient resulted after the inception of boiling, the values are listed only for positive or zero gradients.

Film Boiling Region

Average ribbon temperature. - No attempt was made to predict the ribbon temperatures in the film boiling region, although it appears possible that an analysis of the same type as that employed in the nonboiling region is possible. The problem would be that of heat transfer by conduction, from the ribbon through a film of steam and into an infinite medium.

Upon transition from the nucleate boiling region to the film boiling region, the ribbon temperature rose rapidly and if heating were continued the ribbon would have been destroyed. As shown in figure 5(c), as the degree of subcooling was decreased, the rate of heat absorption approached the rate of heat generation. Thus, at high heat-generation rates and fluid temperatures near saturation, the ribbon temperature corresponded closely to that which would have occurred had the ribbon been completely insulated.

Heat transfer. - In the transition from nucleate to film boiling, the vapor bubbles expanded as previously described until they coalesced. The ribbon was completely surrounded by a number of vapor bubbles which had merged together, although the large individual bubbles were still discernable. Because of the relatively thick layer of bubbles, the rate

of heat transfer was decreased and the ribbon temperature consequently rose. As the temperature continued to rise, the film increased in thickness until a condition of such instability was reached that the film exploded, shooting off bubbles of enormous size relative to the ribbon. A very thin pulsating film in which individual bubbles were no longer discernible immediately formed and the transition to stable film boiling was complete.

Critical Heat Flux

In the region of transition from nucleate to film boiling, there is a maximum rate of heat transfer. This value is usually termed the critical or maximum heat flux.

Experimentally obtained transient critical heat flux values are tabulated in table II. The third to ninth values indicate that for constant heat-generation rate the critical heat flux decreased as the degree of subcooling decreased. The second and eighth or first and ninth values indicate that, for a given degree of subcooling, the critical heat flux increased as the heat-generation rate increased.

The bubble formation in the neighborhood of the critical heat flux corresponding to figures 7(c), 8(c), and 9(c) is illustrated in figure 11. From figure 8(c) it may be seen that q_c occurred at 3 milliseconds. Between 2.9 and 3.1 milliseconds the bubble formation expanded and covered a larger area of the ribbon. The increased coverage of ribbon area by bubble formation offset the turbulence created by the expansion of old bubbles and the formation of new bubbles with the result that the thermal resistance increased and consequently the rate of heat transfer decreased.

SUMMARY OF RESULTS

The following results were obtained from the experimental and analytical investigation of transient water pool boiling resulting from a sudden large power surge:

1. For time periods in the nonboiling region up to 30 milliseconds (the maximum time duration investigated), free-convection effects were negligible and heat transfer therefore occurred by the process of conduction. Thus, ribbon temperatures may be predicted as a function of time and rate of heat generation up to the inception of boiling.

2. For time periods in the nonboiling region of less than 14 milliseconds, the maximum deviation of the average ribbon temperature from that obtained by assuming the ribbon to be completely insulated was 43 percent.

3. In the nucleate boiling region, the average ribbon temperature was 250° F. The deviation from this average was ±16 percent.

4. For heat-generation rates much greater than those required for film boiling, the ribbon temperature was predicted over the entire range (nonboiling and nucleate and film boiling) by the assumption that the ribbon is completely insulated.

5. Transient critical heat flux values up to 3×10^6 Btu per hour per square foot were obtained for water at atmospheric pressure.

a. For a constant heat-generation rate, the critical heat flux increased as the degree of subcooling increased.

b. For a constant degree of subcooling, the critical heat flux increased as the rate of heat generation was increased.

Lewis Flight Propulsion Laboratory
National Advisory Committee for Aeronautics
Cleveland, Ohio, Sept. 17, 1956

APPENDIX A

NOMENCLATURE

A_1, A_2	constants
B_1, B_2	constants
b	value of ordinate on plot of heat-generation rate per unit volume-time, Btu/(hr)(cu ft)
C_1, C_2	constants
c_p	specific heat, Btu/(lb)(°F)
d	heat source, Btu/(hr)(cu ft)
erf	error function
erfc	complementary error function, 1 - erf
h	heat-transfer coefficient, Btu/(hr)(sq ft)(°F)
I	line current, amp
k	thermal conductivity, Btu/((hr)(sq ft)(°F)/ft))
l	length of ribbon, ft
m	slope on heat generation rate per unit volume-time plot, Btu/(hr^2)(cu ft)
n	integer, 1, 2, 3, . . .
P	power or rate of heat generation, Btu/hr
Q	thermal energy generated in a system, Btu
q	thermal energy transferred to a system per unit time per square foot of surface area, Btu/(hr)(sq ft)
q_c	critical heat flux, Btu/(hr)(sq ft)
R	ribbon resistance, ohms
r	$\frac{m + sb}{ks^2}$

S	surface area of ribbon, sq ft
s	variable introduced by application of Laplace transformation. If $f(t)$ is a known function of t for values of $t>0$, its Laplace transform $\bar{f}(s)$ is defined by the equation $\bar{f}(s) = \int_0^\infty e^{-st} f(t)\, dt$ (ref. 5)
T	absolute temperature, $^\circ K$
t	time, hr or millisec as specified
V	volume of ribbon, cu ft
v	voltage drop, volts
w	mass of ribbon, lb
x,y,z	coordinate system, ft
α	thermal diffusivity $\frac{k}{\rho c_p}$, sq ft/hr
β	$k/\alpha^{1/2}$
γ	$\beta_2/(\beta_2 + \beta_1)$
ζ	$(\beta_2 - \beta_1)/(\beta_2 + \beta_1)$
θ	temperature, $^\circ F$
θ_o	initial system temperature, $^\circ F$
θ_{sub}	coolant saturation temperature minus average coolant temperature, $^\circ F$
θ_w	average ribbon temperature, $^\circ F$
$\bar{\theta}$	Laplace transform of θ
μ	$(s/\alpha)^{1/2}$
ρ	density, lb/cu ft
τ	1/2 thickness of ribbon, ft

Subscripts:

1	region of ribbon
2	region of medium surrounding ribbon

APPENDIX B

TEMPERATURE DISTRIBUTION ALONG LENGTH OF RIBBON

This analysis is intended to illustrate the type of temperature distribution (fig. 4) obtainable along an internally heated finite length of ribbon suspended horizontally by means of two copper rods, if the mode of heat transfer is assumed to be solely conduction along its length. The model may be described as follows:

(1) It is an infinite slab of finite length l, and each end is in contact with a heat sink.

(2) The slab has conductivity k, density ρ, specific heat c_p, and a heat source d.

(3) The temperature distribution satisfies the following equations:

$$\frac{\partial^2\theta(x,t)}{\partial x^2} - \frac{\rho c_p}{k}\frac{\partial\theta(x,t)}{\partial t} = -\frac{d}{k} \tag{B1}$$

$$\left.\begin{aligned} &\theta(l,t) = 0 \\ &\left.\frac{\partial\theta}{\partial x}\right]_{x=l/2} = 0 \end{aligned}\right\} \qquad \theta(x,0) = 0 \tag{B2}$$

The experimental data indicate that d may be expressed as a linear function of time. Equation (B1) thus becomes

$$\frac{\partial^2\theta(x,t)}{\partial x^2} - \frac{\rho c_p}{k}\frac{\partial\theta(x,t)}{\partial t} = -\frac{(mt+b)}{k} \tag{B3}$$

Applying the Laplace transformation to equations (B2) and (B3)

$$\frac{d^2\overline{\theta}(x,s)}{dx^2} - \mu^2\overline{\theta}(x,s) = -r \tag{B4}$$

where

$$\mu^2 = \frac{s}{\alpha},\ \alpha = \frac{k}{\rho c_p},\ \text{and}\ \ r = \frac{m+sb}{ks^2}$$

Solving equation (B4) gives

$$\overline{\theta}(x,s) = C_1 e^{-\mu x} + C_2 e^{\mu x} + \frac{r}{\mu^2} \tag{B5}$$

Making use of equations (B2), equation (B5) becomes

$$\overline{\theta}(x,s) = \frac{r}{\mu^2}\left(1 - \frac{e^{-\mu x}}{1 + e^{-\mu l}} - \frac{e^{\mu x}}{1 + e^{\mu l}}\right) \tag{B6}$$

Equation (B6) may be written as (ref. 4)

$$\overline{\theta}(x,s) = \frac{r}{\mu^2}\left\{1 - \left[e^{-\mu x} + e^{-\mu(l-x)}\right]\left[1 + e^{-\mu l}\right]^{-1}\right\} \tag{B7}$$

Expanding the quantity $\left(1 + e^{-\mu l}\right)^{-1}$ yields

$$\left(1 + e^{-\mu l}\right)^{-1} = 1 - e^{-\mu l} + e^{-2\mu l} - \ldots + (-1)^n e^{-\mu n l} = \sum_{n=0}^{\infty} (-1)^n e^{-\mu n l} \tag{B8}$$

where $n = 0,1,2,\ldots$ and $e^{-2\mu l} < 1$

Substituting equation (B8) in equation (B7) results in

$$\overline{\theta}(x,s) = \frac{r}{\mu^2}\left\{1 - \left[e^{-\mu x} + e^{-\mu(l-x)}\right]\sum_{n=0}^{\infty} (-1)^n e^{-\mu l n}\right\} \tag{B9}$$

Expanding equation (B9) and substituting for r

$$\overline{\theta}(x,s) = \frac{\alpha}{ks^2}\left(\frac{m}{s} + b\right)\left\{1 - \sum_{n=0}^{\infty} (-1)^n e^{-\mu(nl+x)} - \sum_{n=0}^{\infty} (-1)^n e^{-\mu\left[l(n+1)-x\right]}\right\} \tag{B10}$$

Taking the inverse transform and simplifying yields

$$\theta(x,t) = \frac{\alpha t}{2k}(mt + 2b) - \frac{16\alpha m t^2}{k}\left\{i^4\mathrm{erfc}\,\frac{x}{2\sqrt{\alpha t}} + \sum_{n=1}^{\infty} (-1)^{n+1}\left[i^4\mathrm{erfc}\,\frac{nl - x}{2\sqrt{\alpha t}} - i^4\mathrm{erfc}\,\frac{nl + x}{2\sqrt{\alpha t}}\right]\right\} - \frac{4\alpha b t}{k}\left\{i^2\mathrm{erfc}\,\frac{x}{2\sqrt{\alpha t}} + \sum_{n=1}^{\infty} (-1)^{n+1}\left[i^2\mathrm{erfc}\,\frac{nl - x}{2\sqrt{\alpha t}} - i^2\mathrm{erfc}\,\frac{nl + x}{2\sqrt{\alpha t}}\right]\right\} \tag{B11}$$

APPENDIX C

SIMPLIFIED DERIVATION OF RIBBON TEMPERATURE

It is assumed that during short time periods, heat transfer from the ribbon can be neglected in the nonboiling region and, therefore, that the rate of heat absorption equals the rate of heat generation; the ribbon is completely insulated.

$$\frac{d(Q/V)}{dt} = \rho c_p \frac{d\theta_w}{dt} \tag{C1}$$

Equation (C1) may be written in integral form as

$$\int_0^t \frac{d(Q/V)}{dt}\,dt = \rho c_p \int_{\theta_o}^{\theta_w} d\theta_w \tag{C2}$$

The ribbon temperature may be evaluated from equation (C2) by determining the area under the curve resulting from a plot of $d(Q/V)/dt$ against t.

The heat-generation rates obtained experimentally from a step change in voltage were found to be representable as a linear function of time, that is,

$$\frac{d(Q/V)}{dt} = mt + b \tag{C3}$$

Substituting equation (C3) into equation (C2) gives

$$\int_{\theta_o}^{\theta_w} d\theta_w = \frac{1}{\rho c_p}\int_0^t (mt + b)dt \tag{C4}$$

Assuming ρ and c_p constant, equation (C4) becomes upon integrating

$$\theta_w = \theta_o + \frac{t}{2\rho c_p}(mt + 2b) \tag{C5}$$

APPENDIX D

TEMPERATURE DISTRIBUTION THROUGH RIBBON INTO AN INFINITE MEDIUM

This analysis is intended to illustrate the type of temperature distributions (figs. 5(a) and (b)) obtainable along the finite thickness of an internally heated ribbon in contact with an infinite medium, if the mode of heat transfer is assumed to be conduction through the ribbon and into the surrounding medium. The ribbon may be described as follows:

1. It is an infinite slab of finite thickness in contact with an infinite medium.

2. The slab (region 1) has conductivity k_1, density ρ_1, specific heat $c_{p,1}$, and a heat source d.

3. The infinite medium (region 2) has corresponding constants k_2, ρ_2, and $c_{p,2}$ and no heat source.

4. The temperature distributions, $\theta_1(y,t)$ and $\theta_2(y,t)$, satisfy the following equations:

$$\frac{\partial^2\theta_1(y,t)}{\partial y^2} - \frac{\rho_1 c_{p,1}}{k_1}\frac{\partial\theta_1(y,t)}{\partial t} = -\frac{d}{k_1} \qquad 0 \le y < \tau \tag{D1}$$

$$\frac{\partial^2\theta_2(y,t)}{\partial y^2} - \frac{\rho_2 c_{p,2}}{k_2}\frac{\partial\theta_2(y,t)}{\partial t} = 0 \qquad y > \tau \tag{D2}$$

$$\left.\begin{aligned} \theta_1(\tau,t) &= \theta_2(\tau,t) \\ \left(k_1\frac{\partial\theta_1}{\partial y}\right)_{y=\tau} &= \left(k_2\frac{\partial\theta_2}{\partial y}\right)_{y=\tau} \end{aligned}\right\} \tag{D3}$$

$$\left.\begin{aligned} \left(\frac{\partial\theta_1}{\partial y}\right)_{y=0} &= 0 \\ \lim_{y\to\infty}\theta_2 &= 0 \end{aligned}\right\} \tag{D4}$$

The experimental data indicate that d may be expressed as a linear function of time. Equation (D1) thus becomes

$$\frac{\partial^2\theta_1(y,t)}{\partial y^2} - \frac{\rho_1 c_{p,1}}{k_1}\frac{\partial\theta_1(y,t)}{\partial t} = -\frac{1}{k_1}(mt + b) \qquad 0 \le y < \tau \tag{D5}$$

Applying the Laplace transformation to equations (D2), (D3), (D4), and (D5) results in

$$\frac{d^2\overline{\theta}_1(y,s)}{dy^2} - \mu_1^2\,\overline{\theta}_1(y,s) = -r \tag{D6}$$

$$\frac{d^2\overline{\theta}_2(y,s)}{dy^2} - \mu_2^2\,\overline{\theta}_2(y,s) = 0 \tag{D7}$$

where

$$\mu_{1,2}^2 = \frac{s}{\alpha_{1,2}}, \quad \alpha_{1,2} = \frac{k_{1,2}}{\rho_{1,2}c_{p,1,2}}, \quad \text{and} \quad r = \frac{m + sb}{k_1 s^2}$$

The solutions of equations (D6) and (D7) may be written

$$\overline{\theta}(y,s) = A_1(s)e^{-\mu_1 y} + B_1(s)e^{\mu_1 y} + \frac{r}{\mu_1^2} \tag{D8}$$

$$\overline{\theta}_2(y,s) = A_2(s)e^{-\mu_2 y} + B_2(s)e^{\mu_2 y} \tag{D9}$$

By use of equations (D4), equations (D8) and (D9) become

$$\overline{\theta}_1(y,s) = A_1(s)\left(e^{\mu_1 y} + e^{-\mu_1 y}\right) + \frac{r}{\mu_1^2} \tag{D10}$$

$$\overline{\theta}_2(y,s) = A_2(s)e^{-\mu_2 y} \tag{D11}$$

Making use of the boundary conditions in equations (D3), the constants A_1 and A_2 in equations (D10) and (D11) are found to be

$$A_1 = -\frac{rk_2\mu_2}{\mu_1^2}\left[\mu_2 k_2(e^{\mu_1\tau} + e^{-\mu_1\tau}) + \mu_1 k_1(e^{\mu_1\tau} - e^{-\mu_1\tau})\right]^{-1} \tag{D12}$$

$$A_2 = \frac{rk_1}{\mu_1}\frac{\left(e^{\mu_1\tau} - e^{-\mu_1\tau}\right)}{e^{-\mu_2\tau}}\left[\mu_2 k_2(e^{\mu_1\tau} + e^{-\mu_1\tau}) + \mu_1 k_1(e^{\mu_1\tau} - e^{-\mu_1\tau})\right]^{-1} \tag{D13}$$

Substituting equations (D12) and (D13) into equations (D10) and (D11) results in

$$\bar{\theta}_1(y,s) = \frac{r}{\mu_1^2}\left\{1 - k_2\mu_2\left[\frac{e^{\mu_1 y} + e^{-\mu_1 y}}{\mu_2 k_2(e^{\mu_1\tau} + e^{-\mu_1\tau}) + \mu_1 k_1(e^{\mu_1\tau} - e^{-\mu_1\tau})}\right]\right\} \tag{D14}$$

$$\bar{\theta}_2(y,s) = \frac{rk_1}{\mu_1}\left(\frac{e^{-\mu_2 y}}{e^{-\mu_2\tau}}\right)\left[\frac{e^{\mu_1\tau} - e^{-\mu_1\tau}}{\mu_2 k_2(e^{\mu_1\tau} + e^{-\mu_1\tau}) + \mu_1 k_1(e^{\mu_1\tau} - e^{-\mu_1\tau})}\right] \tag{D15}$$

Simplifying equations (D14) and (D15) gives the equations

$$\bar{\theta}_1(y,s) = \frac{r\alpha_1}{s}\left\{1 - \frac{\beta_2}{\beta_2 + \beta_1}\left[e^{-\mu_1(\tau-y)} + e^{-\mu_1(\tau+y)}\right]\left(1 + \zeta e^{-2\mu_1\tau}\right)^{-1}\right\} \tag{D16}$$

$$\bar{\theta}_2(y,s) = \frac{rk_1\alpha_1^{1/2}}{s(\beta_2 + \beta_1)}\, e^{-\mu_2(y-\tau)}\left(1 - e^{-2\mu_1\tau}\right)\left(1 + \zeta e^{-2\mu_1\tau}\right)^{-1} \tag{D17}$$

where

$$\beta_{1,2} = \frac{k_{1,2}}{\alpha_{1,2}^{1/2}}, \quad \text{and} \quad \zeta = \frac{\beta_2 - \beta_1}{\beta_2 + \beta_1}$$

Expanding the quantity $\left(1 + \zeta e^{-2\mu_1\tau}\right)^{-1}$ yields

$$\left(1 + \zeta e^{-2\mu_1\tau}\right)^{-1} = 1 - \zeta e^{-2\mu_1\tau} + \zeta^2 e^{-4\mu_1\tau} - \ldots + (-1)^n \zeta^n e^{-2\mu_1\tau n} = \sum_{n=0}^{\infty} (-1)^n \zeta^n e^{-2\mu_1\tau n} \tag{D18}$$

for $n = 0,1,2,\ldots$ and $\zeta^2 e^{-4\mu_1\tau} < 1$

Equations (D16) and (D17) then become

$$\overline{\theta}_1(y,s) = \frac{r\alpha_1}{s}\left\{1 - \gamma\left[e^{-\mu_1(\tau-y)} + e^{-\mu_1(\tau+y)}\right]\sum_{n=0}^{\infty}(-1)^n \zeta^n e^{-2\mu_1\tau n}\right\} \tag{D19}$$

$$\overline{\theta}_2(y,s) = \frac{rk_1\alpha_1^{1/2}}{s(\beta_2+\beta_1)}\left\{\left[e^{-\mu_2(y-\tau)} - e^{-\mu_2(y-\tau)-2\mu_1\tau}\right]\sum_{n=0}^{\infty}(-1)^n \zeta^n e^{-2\mu_1\tau n}\right\} \tag{D20}$$

where $\gamma = \dfrac{\beta_2}{\beta_2+\beta_1}$

Expanding, taking the inverse transform, and simplifying equations (D19) and (D20) result in

$$\theta_1(y,t) = \frac{\alpha_1 t}{2k_1}(mt + 2b) - \frac{16\alpha_1 mt^2\gamma}{k_1}\left(\sum_{n=0}^{\infty}(-1)^n\zeta^n\left\{i^4\operatorname{erfc}\frac{[\tau(2n+1)-y]}{2\sqrt{\alpha_1 t}} + i^4\operatorname{erfc}\frac{[\tau(2n+1)+y]}{2\sqrt{\alpha_1 t}}\right\}\right) - \frac{4\alpha_1 bt\gamma}{k_1}\left(\sum_{n=0}^{\infty}(-1)^n\zeta^n\left\{i^2\operatorname{erfc}\frac{[\tau(2n+1)-y]}{2\sqrt{\alpha_1 t}} + i^2\operatorname{erfc}\frac{[\tau(2n+1)+y]}{2\sqrt{\alpha_1 t}}\right\}\right) \tag{D21}$$

$$\theta_2(y,t) = \frac{\alpha_1^{1/2}}{\beta_2+\beta_1}\left(m\sum_{n=0}^{\infty}(-1)^n\zeta^n(4t)^2\left\{i^4\operatorname{erfc}\frac{\left[\alpha_1^{1/2}(y-\tau) + 2\alpha_2^{1/2}\tau n\right]}{2\sqrt{\alpha_2\alpha_1 t}} - i^4\operatorname{erfc}\frac{\left[\alpha_1^{1/2}(y-\tau) + 2\alpha_2^{1/2}\tau(n+1)\right]}{2\sqrt{\alpha_2\alpha_1 t}}\right\} + b\sum_{n=0}^{\infty}(-1)^n\zeta^n(4t)\left\{i^2\operatorname{erfc}\frac{\left[\alpha_1^{1/2}(y-\tau) + 2\alpha_2^{1/2}\tau n\right]}{2\sqrt{\alpha_2\alpha_1 t}} - i^2\operatorname{erfc}\frac{\left[\alpha_1^{1/2}(y-\tau) + 2\alpha_2^{1/2}\tau(n+1)\right]}{2\sqrt{\alpha_2\alpha_1 t}}\right\}\right) \tag{D22}$$

APPENDIX E

AVERAGE RIBBON TEMPERATURE

The equations developed in appendix D for the temperature distributions may be integrated as follows to yield an equation representing the average ribbon temperature:

$$\bar{\theta}_w = \frac{1}{\tau} \int_0^{\tau} \bar{\theta}_1(y,s)\, dy \tag{E1}$$

Substituting equation (D19) into equation (E1) gives

$$\bar{\theta}_w = \frac{r\alpha_1}{s\tau} \int_0^{\tau} \left\{ 1 - \gamma \left[e^{-\mu_1(\tau-y)} + e^{-\mu_1(\tau+y)} \right] \sum_{n=0}^{\infty} (-1)^n \zeta^n\, e^{-2\mu_1 \tau n} \right\} dy \tag{E2}$$

Integrating and simplifying equation (E2) yield

$$\bar{\theta}_w = \frac{r\alpha_1}{s\tau} \left\{ \tau - \frac{\gamma}{\mu_1} \sum_{n=0}^{\infty} (-1)^n \zeta^n \left(e^{-2\mu_1 n\tau} - e^{-2\mu_1 \tau (n+1)} \right) \right\} \tag{E3}$$

Substituting for r, taking the inverse transform, and simplifying result in

$$\begin{aligned} \theta_w = {} & \frac{\alpha_1 t}{2k_1} (mt + 2b) - \frac{\gamma \alpha_1^{3/2}}{k_1 \tau} \left\{ m \left[\sum_{n=0}^{\infty} (-1)^n \zeta^n (4t)^{5/2}\, i^5 \operatorname{erfc} \frac{2n\tau}{2\sqrt{\alpha_1 t}} - \right. \right. \\ & \left. \sum_{n=0}^{\infty} (-1)^n \zeta^n (4t)^{5/2}\, i^5 \operatorname{erfc} \frac{2\tau(n+1)}{2\sqrt{\alpha_1 t}} \right] + \\ & b \left[\sum_{n=0}^{\infty} (-1)^n \zeta^n (4t)^{3/2}\, i^3 \operatorname{erfc} \frac{2n\tau}{2\sqrt{\alpha_1 t}} - \right. \\ & \left. \left. \sum_{n=0}^{\infty} (-1)^n \zeta^n (4t)^{3/2}\, i^3 \operatorname{erfc} \frac{2\tau(n+1)}{2\sqrt{\alpha_1 t}} \right] \right\} \end{aligned} \tag{E4}$$

REFERENCES

1. Glasstone, Samuel: Principles of Nuclear Reactor Engineering. D. Van Nostrand Co., Inc., 1955.

2. Perry, John H., ed.: Chemical Engineers' Handbook. Third ed., McGraw-Hill Book Co. Inc., 1950, p. 222.

3. Rosenthal, M. W. (John E. Viscardi, ed.): Transient Boiling Investigation. Rep. NDA-7, Boiling Burnout Newsletter No. 4, Nuclear Dev. Assoc., May 15, 1955. (Contract AT(30-1)862.)

4. Carslaw, H. S. and Jeager, J. C.: Conduction of Heat in Solids. Univ. Press (Oxford), 1947, pp. 251; 380.

5. Thomson, William Tyrell: Laplace Transformation. Prentice-Hall, Inc., 1950.

TABLE I. - NUCLEATE BOILING HEAT-TRANSFER COEFFICIENTS

Initial temperature, θ_o, °F	Average ribbon temperature minus initial system temperature, $\theta_w - \theta_o$, °F	Heat-transfer coefficient, h, $\frac{Btu}{(hr)(sq\ ft)(^oF)}$	Heat flux, q, $\frac{Btu}{(hr)(sq\ ft)}$	Temperature gradient, $d\theta_w/dt$, °F/hr	Heat-generation rate, $\frac{d(Q/S)}{dt}$, $\frac{Btu}{(hr)(sq\ ft)}$
146	90	2170	1.95×10^5	0.756×10^7	2.92×10^5
↓	92	2220	2.04	.684	↓
	94	2270	2.13	.612	
	96	2320	2.23	.540	
	98	2580	2.53	.270	
166	63	3100	1.95	.810	2.985
↓	66	3590	2.37	.468	2.967
	70	3600	2.63	.234	2.930
186	51	1530	.78	1.925	3.26
↓	58	3670	2.13	.810	3.17
	65	4010	2.61	.396	3.12
	69	4400	3.04	.000	3.04
203	37	3570	1.32	1.640	3.43
↓	43	5720	2.46	.684	3.34
	47	6620	3.11	.126	3.27
76	149	3950	5.89	3.24	10.03
↓	156	4630	7.23	2.16	10.00
	163	5200	8.48	1.12	9.93
95	129	3880	5.00	4.50	10.75
↓	139	4650	6.46	3.24	10.62
	144	5320	7.66	2.05	10.30
	151	5660	8.55	1.30	10.22
	153	5960	9.11	.09	10.27
105	117	4000	4.68	4.29	10.14
↓	129	5120	6.60	2.63	9.98
	134	6170	8.28	1.30	9.95
125	97	4210	4.09	5.11	10.57
↓	107	4900	5.24	4.10	10.46
	120	4980	5.98	3.34	10.27
137	86	4090	3.52	5.61	10.67
↓	98	5800	5.68	3.74	10.49
	106	6900	7.32	2.41	10.42
148	68	3930	2.67	6.225	10.57
↓	81	4950	4.01	4.930	10.32
	97	6240	6.24	3.025	10.14
	101	9900	10.00	.000	10.00
185	43	2840	1.22	7.31	10.57
↓	65	8720	5.67	7.42	10.10
	68	11420	7.77	1.80	10.00
77	166	9030	15.0	11.10	29.3
↓	184	14120	26.0	2.36	29.1
	187	15130	28.3	.40	28.8
95	160	6620	10.6	14.70	29.6
↓	194	12920	25.1	3.35	29.5
	198	14500	28.4	.43	29.0
113	115	11120	12.80	12.6	28.9
↓	152	11500	17.47	8.5	28.6
	169	16670	28.20	.0	28.2
131	119	13720	16.32	8.14	26.85
↓	133	19700	26.20	.27	26.55
149	92	17800	16.35	8.64	27.45
↓	112	21000	23.47	2.83	27.15
	116	21600	25.10	1.57	27.15
167	108	6940	7.50	12.88	24.4
↓	138	9520	13.12	8.10	23.9
	153	10150	15.52	5.66	23.1
185	68	10120	6.88	14.05	25.1
↓	100	16400	16.40	6.03	24.3
203	47	10390	4.88	15.05	24.35
↓	80	11100	8.88	11.11	23.50
	111	13900	15.43	5.52	22.50

TABLE II. - CRITICAL HEAT FLUX

Critical heat flux, q_c, $\frac{\text{Btu}}{(\text{hr})(\text{sq ft})}$	Average ribbon temperature minus initial system temperature, $\theta_w - \theta_o$, $^\circ F$	Coolant saturation temperature minus average coolant temperature, θ_{sub}, $^\circ F$	Heat-generation rate, $\frac{d(Q/S)}{dt}$, $\frac{\text{Btu}}{(\text{hr})(\text{sq ft})}$
3.11×10^5	47	9	3.27×10^5
7.77	68	27	10.00
28.30	187	135	28.80
28.20	169	99	28.20
26.20	133	81	26.20
25.10	116	63	27.20
21.00	165	45	23.0
16.40	100	27	24.3
15.43	111	9	22.8

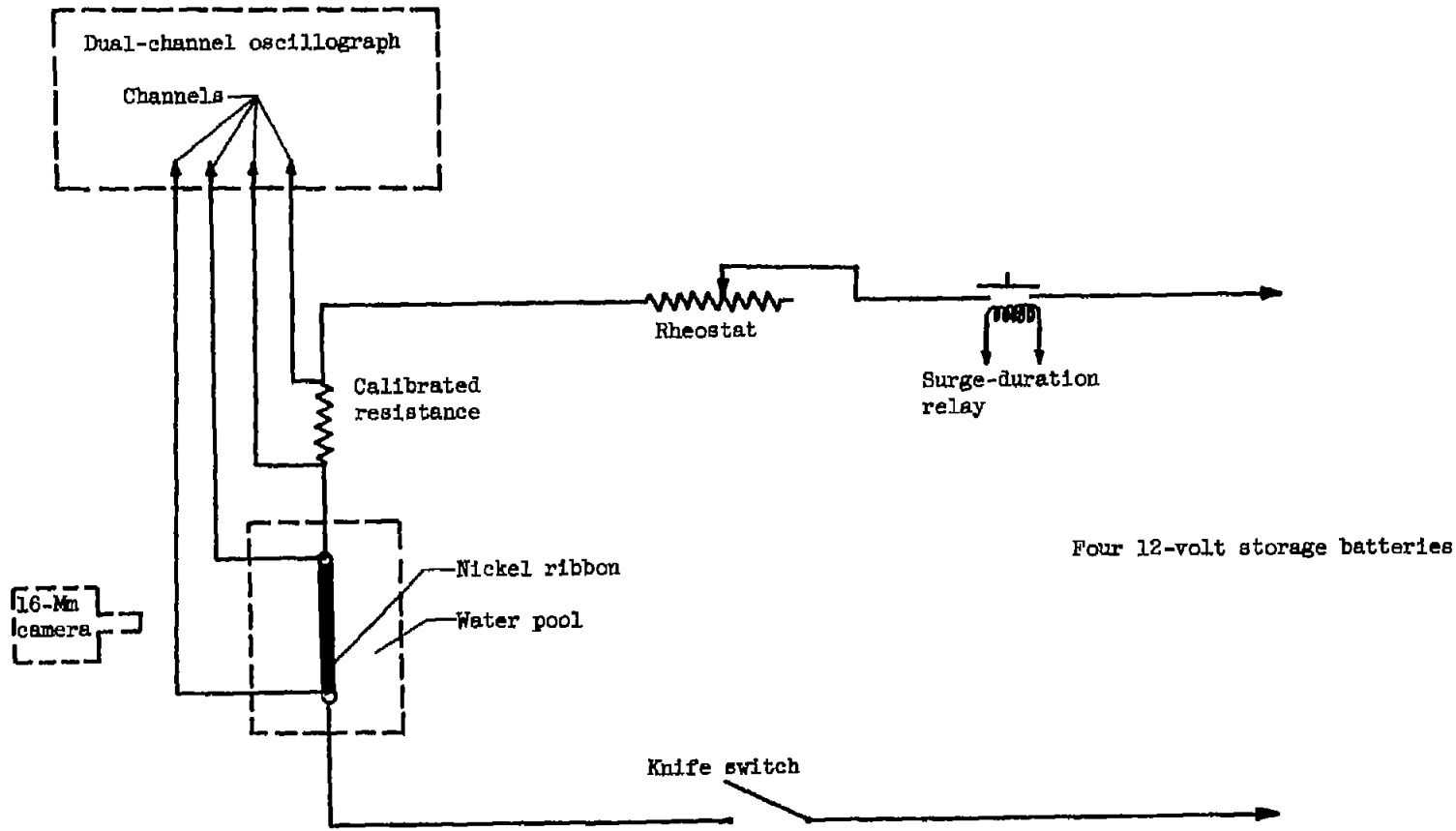

Figure 1. - Schematic diagram of main circuit.

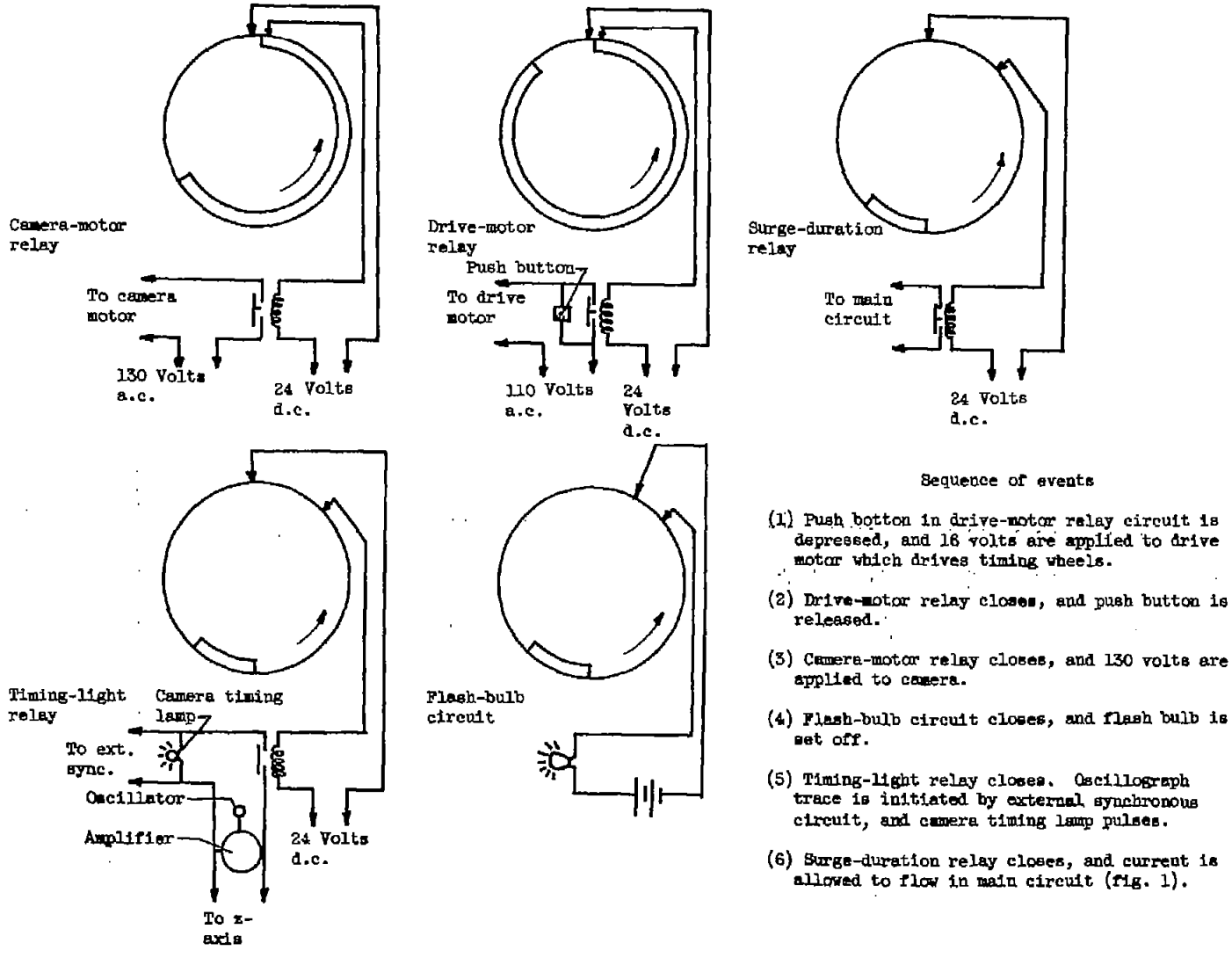

Sequence of events

(1) Push button in drive-motor relay circuit is depressed, and 16 volts are applied to drive motor which drives timing wheels.

(2) Drive-motor relay closes, and push button is released.

(3) Camera-motor relay closes, and 130 volts are applied to camera.

(4) Flash-bulb circuit closes, and flash bulb is set off.

(5) Timing-light relay closes. Oscillograph trace is initiated by external synchronous circuit, and camera timing lamp pulses.

(6) Surge-duration relay closes, and current is allowed to flow in main circuit (fig. 1).

Figure 2. - Schematic diagram of timing wheels and circuits.

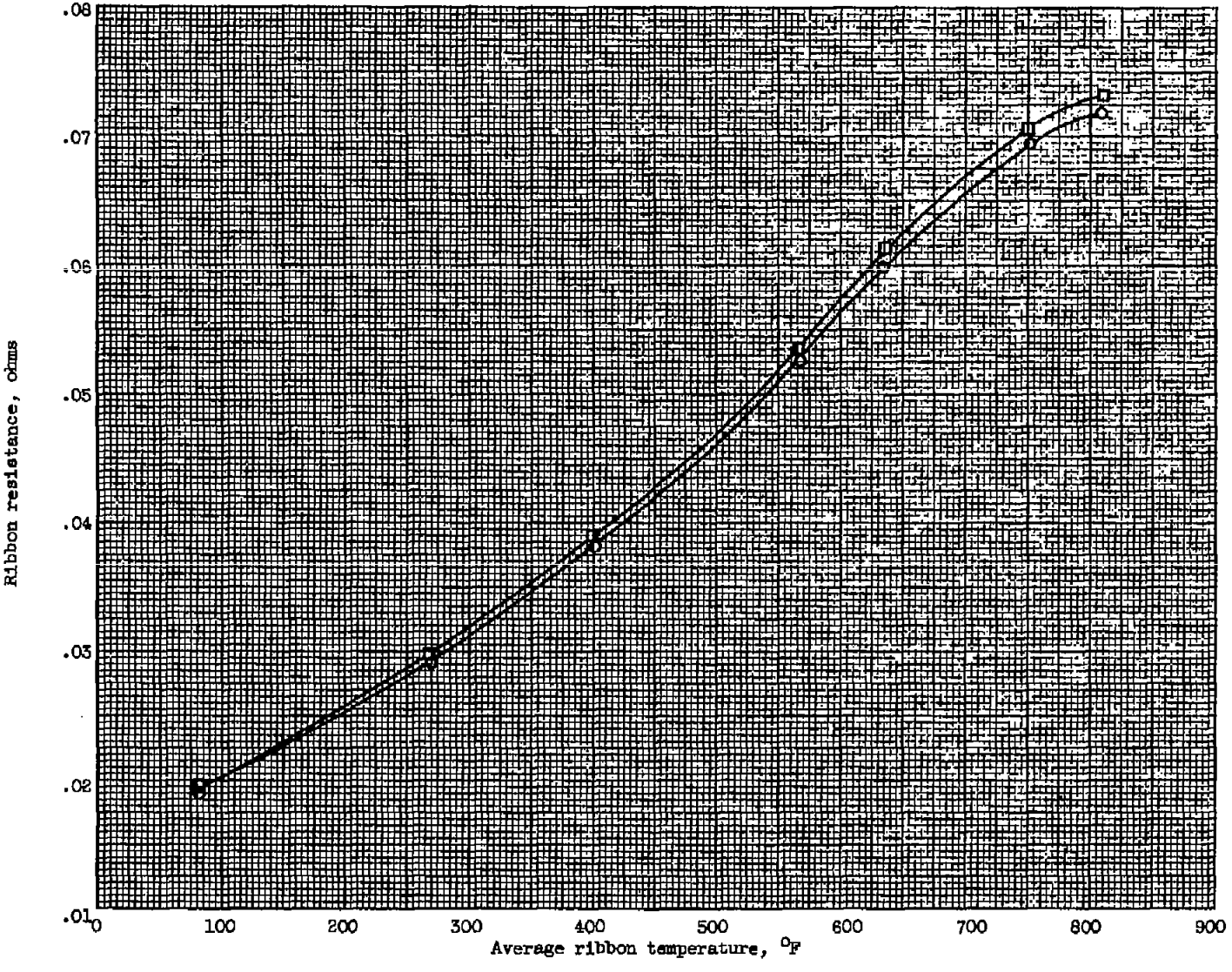

Figure 3. - Resistance-temperature calibration curves for two nickel ribbons.

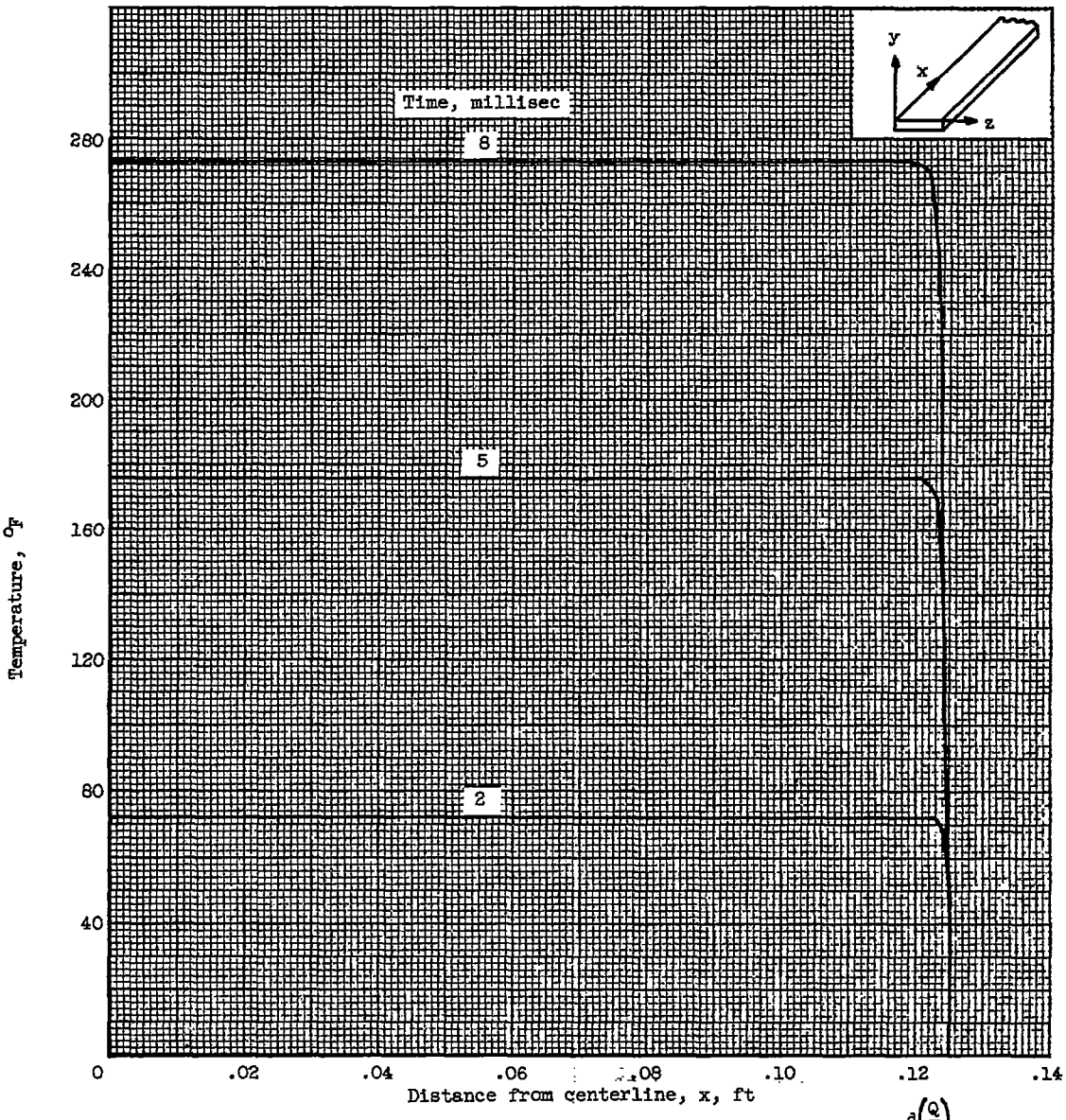

Figure 4. - Temperature gradient along x-axis for heat-generation rate $\frac{d\left(\frac{Q}{V}\right)}{dt}$ of $(-5\times10^{14})t + 8\times10^{9}$ Btu per hour per cubic foot. (See appendix B.)

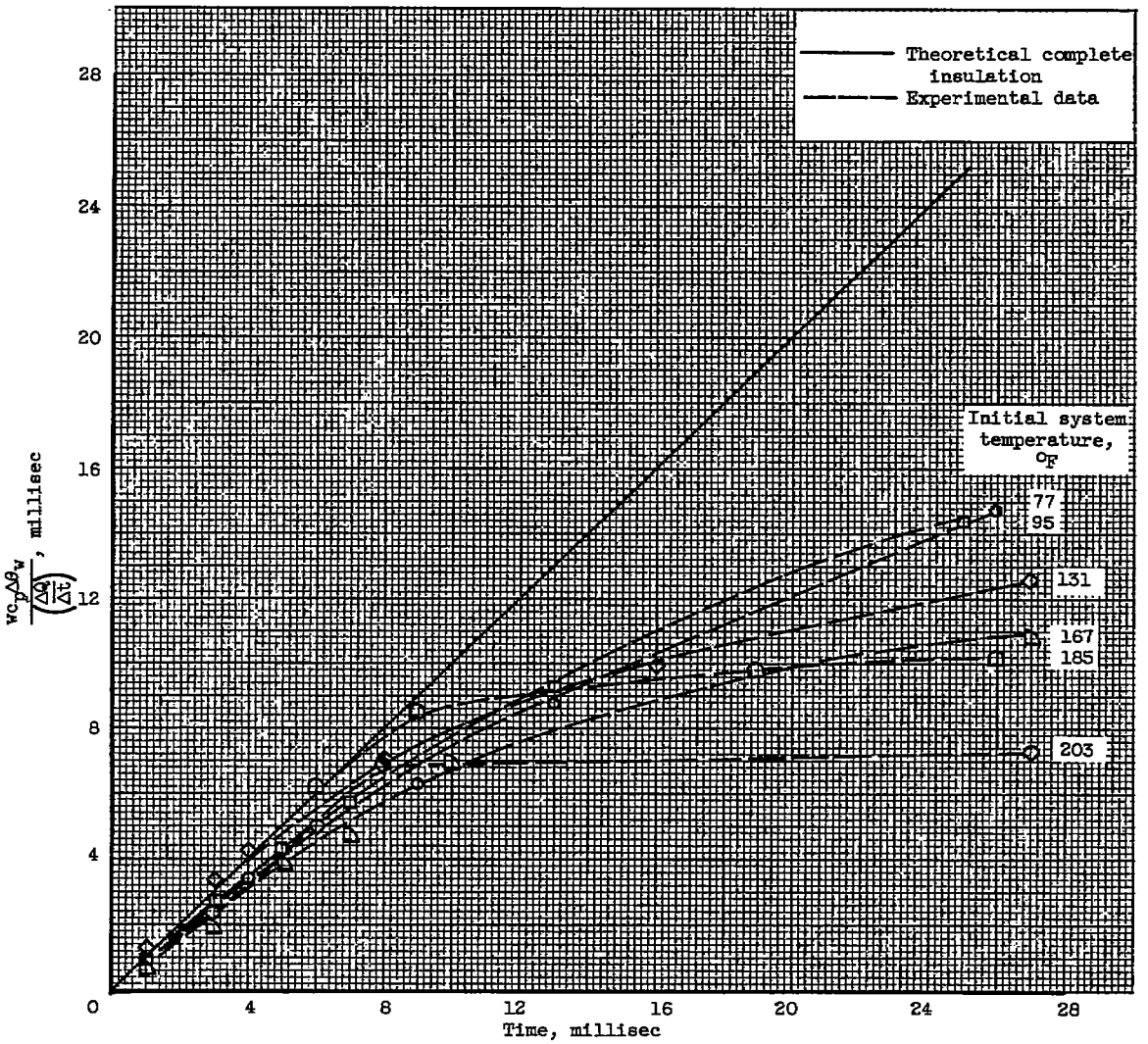

(a) Average heat-generation rate, 3×10^5 Btu per hour per square foot.

Figure 5. - Deviation of experimental data from that obtainable for complete insulation.

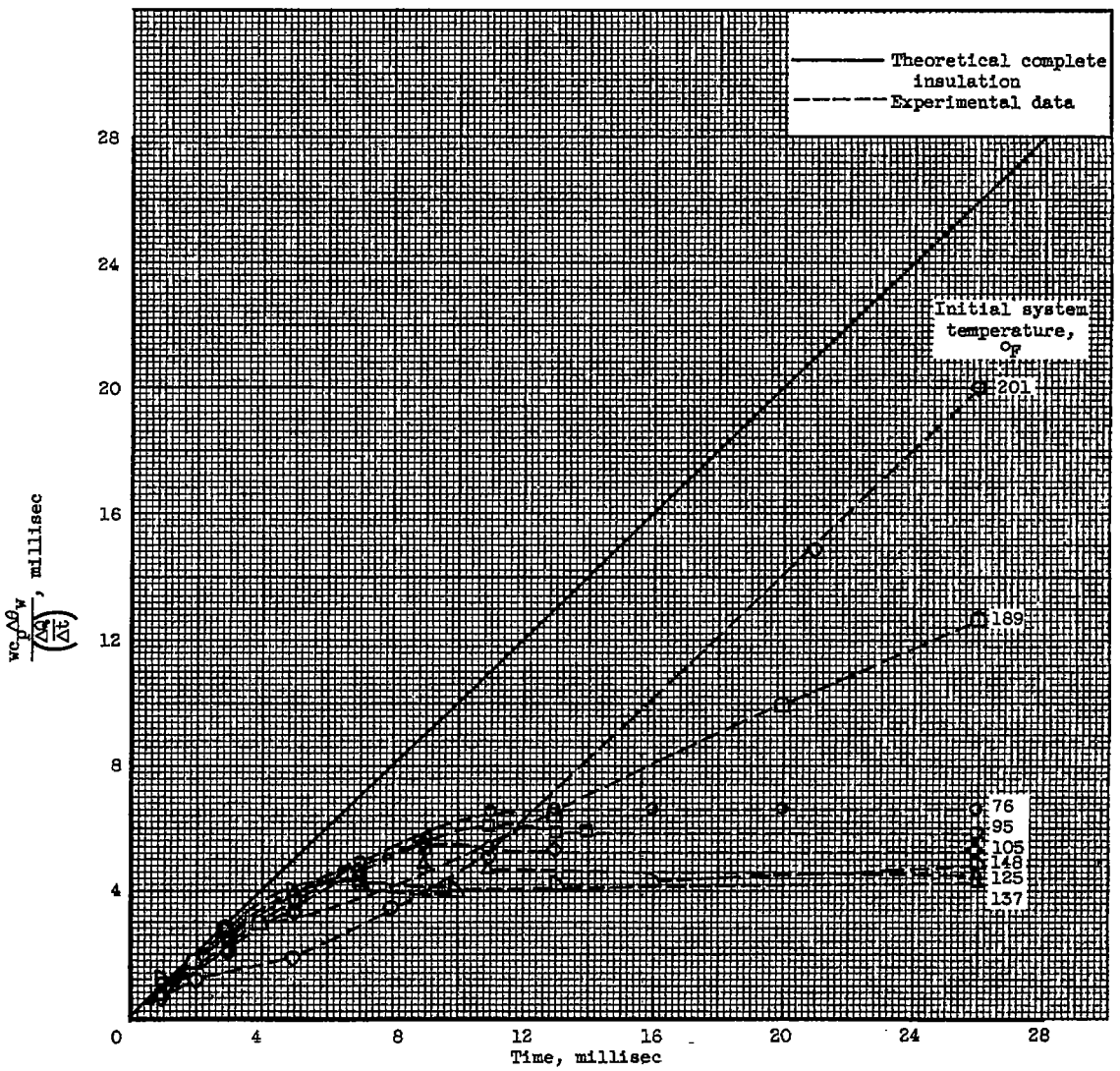

(b) Average heat-generation rate, 10×10^5 Btu per hour per square foot.

Figure 5. - Continued. Deviation of experimental data from that obtainable for complete insulation.

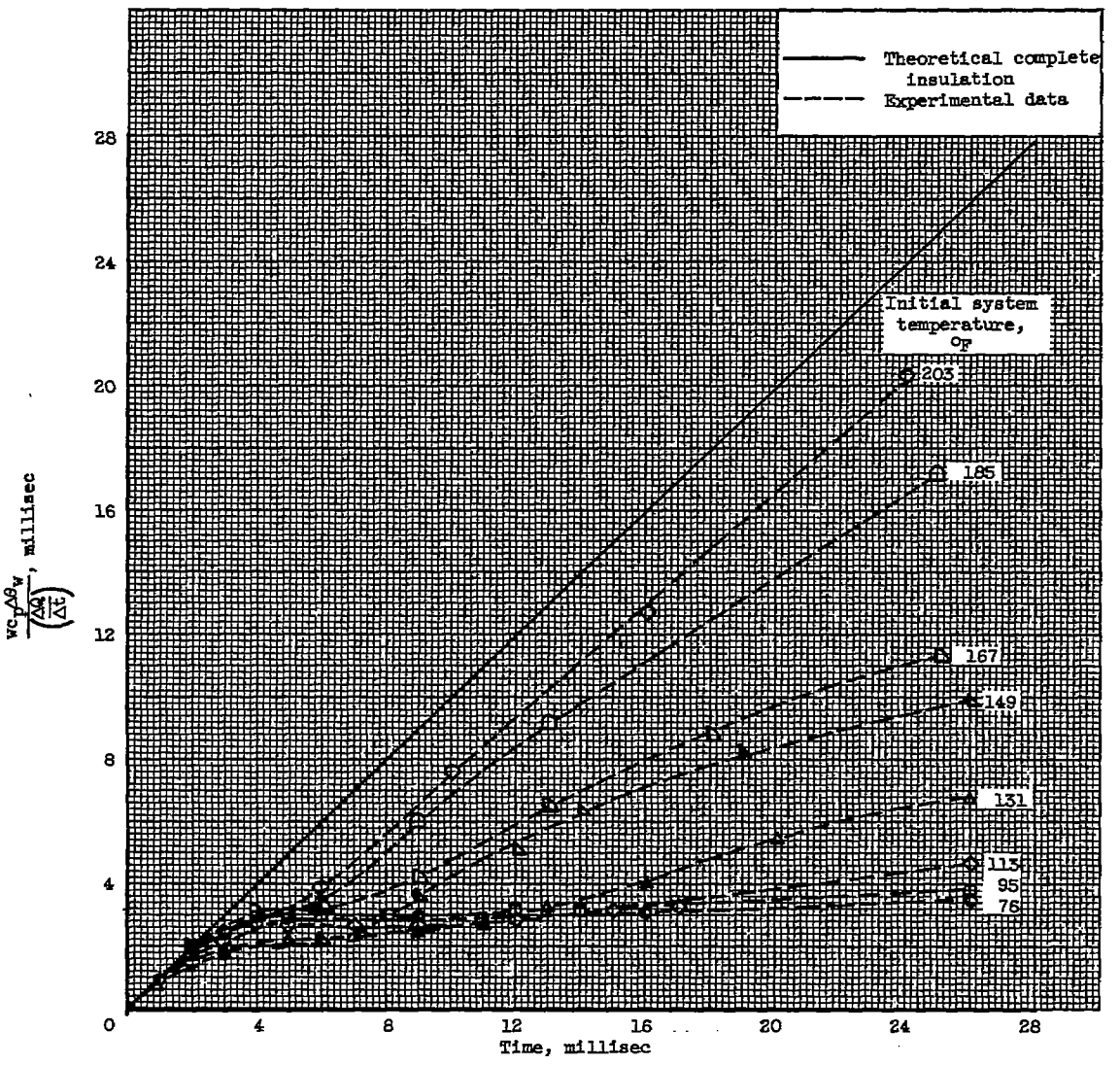

(c) Average heat-generation rate, 20×10^5 Btu per hour per square foot.

Figure 5. - Concluded. Deviation of experimental data from that obtainable for complete insulation.

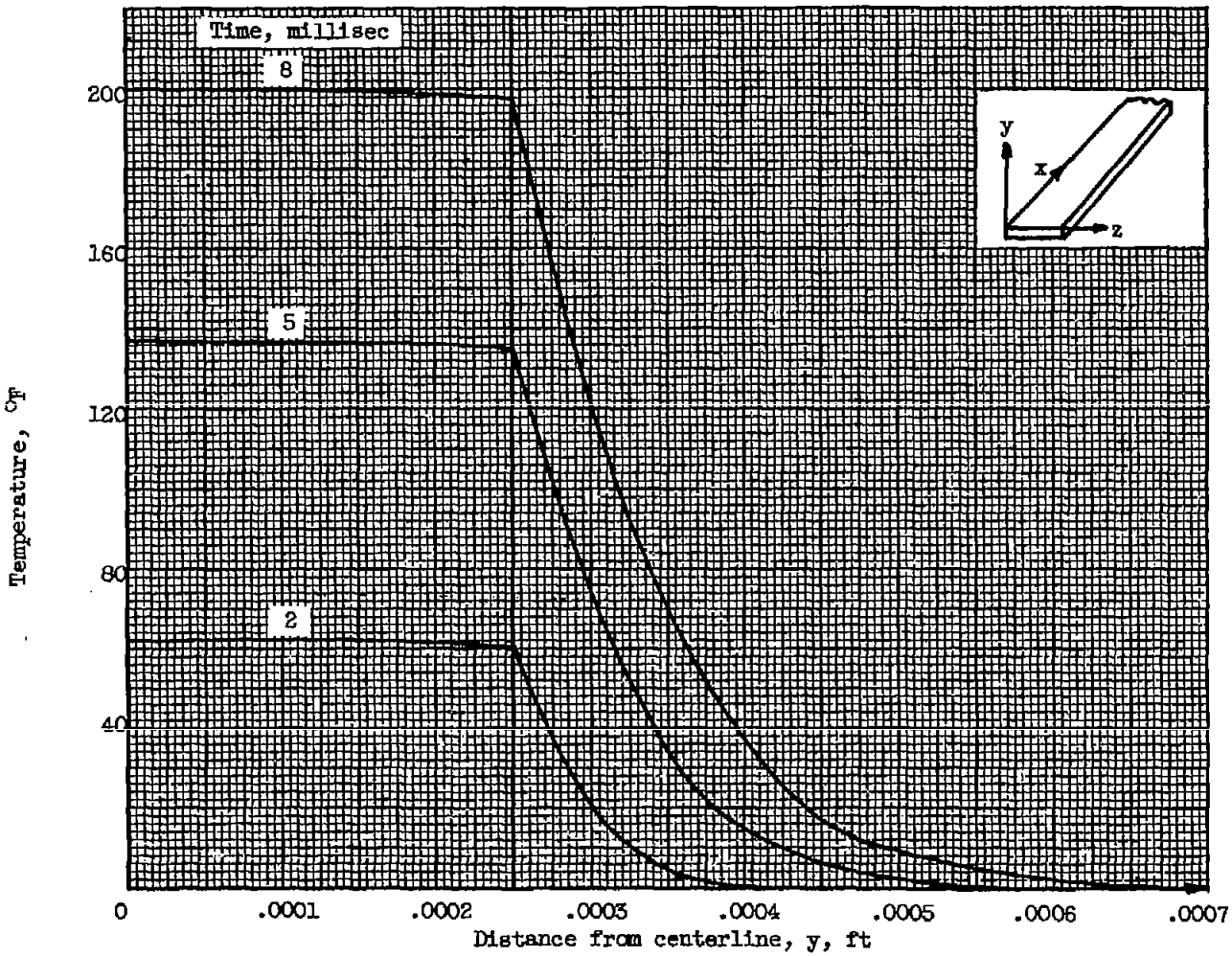

Figure 6. - Temperature gradient along y-axis for heat generation rate $\frac{d\left(\frac{Q}{V}\right)}{dt}$ of $(-5\times10^{14})t + 8\times10^{9}$ Btu per hour per cubic foot. (See appendix B.)

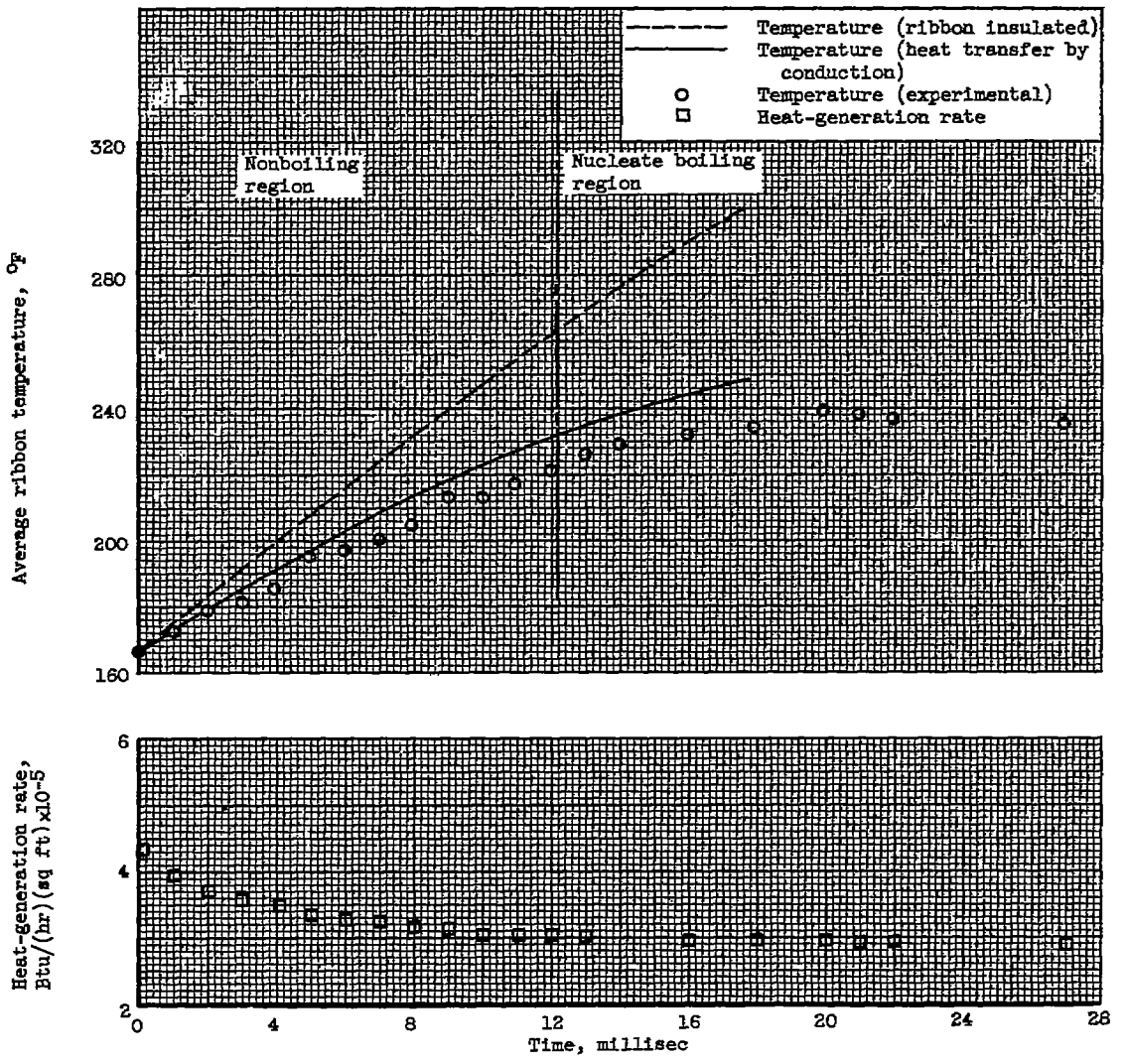

(a) Water temperature, 166° F.

Figure 7. - Temperature - heat-generation-rate - time record for nickel ribbon in subcooled water.

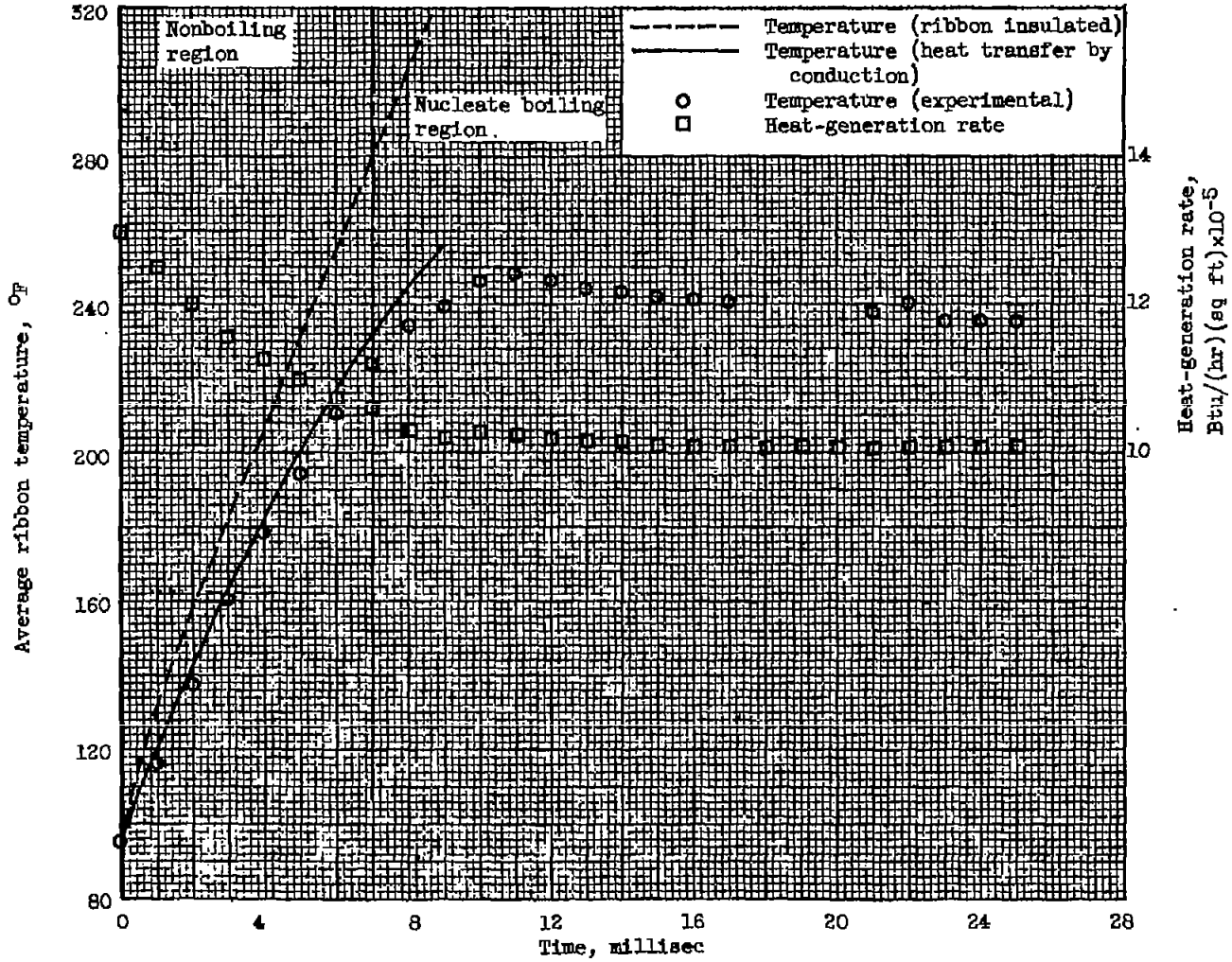

(b) Water temperature, 95° F.

Figure 7. - Continued. Temperature - heat-generation-rate - time record for nickel ribbon in subcooled water.

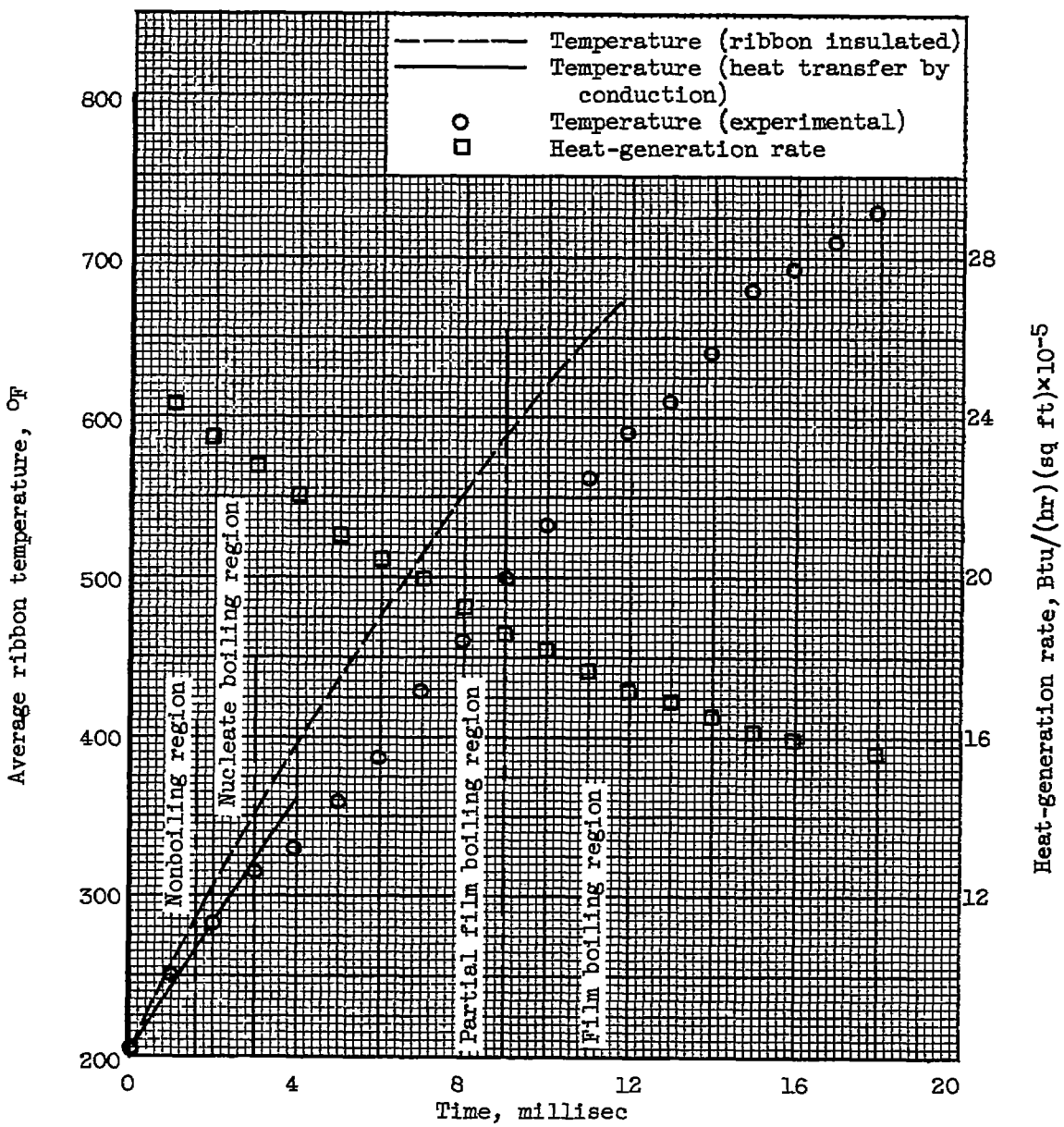

(c) Water temperature, 203° F.

Figure 7. - Concluded. Temperature - heat-generation-rate - time record for nickel ribbon in subcooled water.

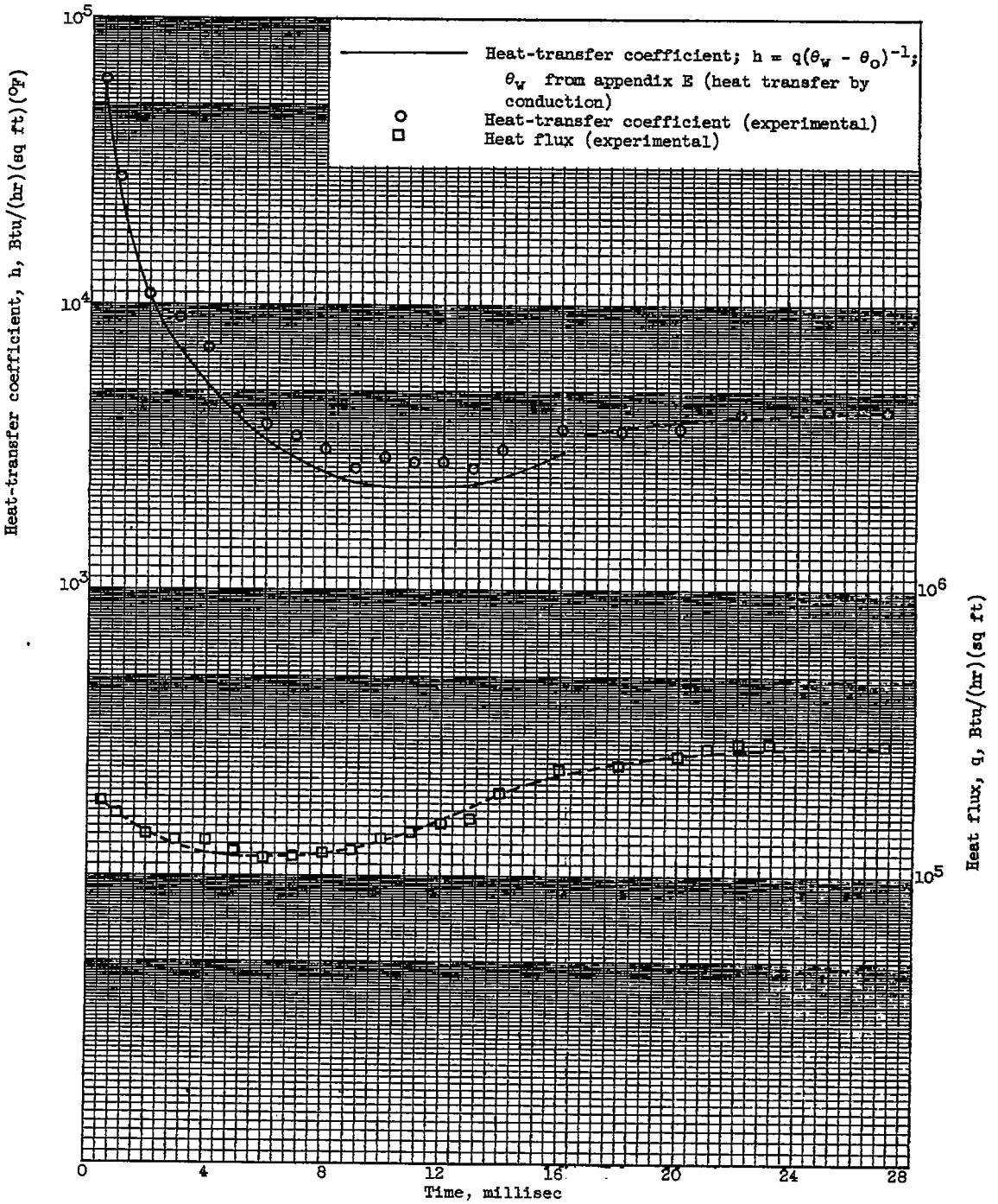

(a) Water temperature, 166° F.

Figure 8. - Heat flux and coefficient of heat transfer against time.

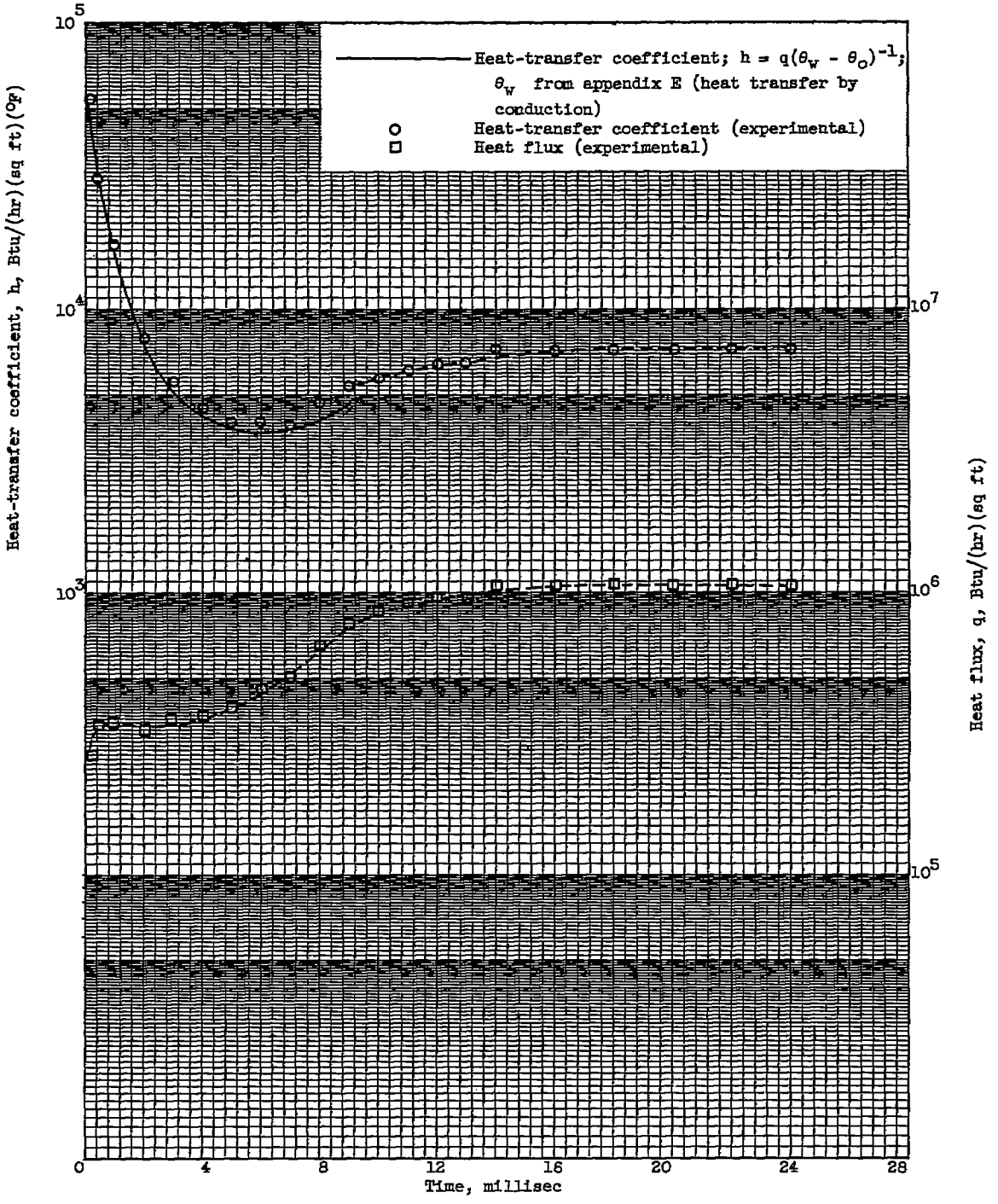

(b) Water temperature, 95° F.

Figure 8. - Continued. Heat flux and coefficient of heat transfer against time.

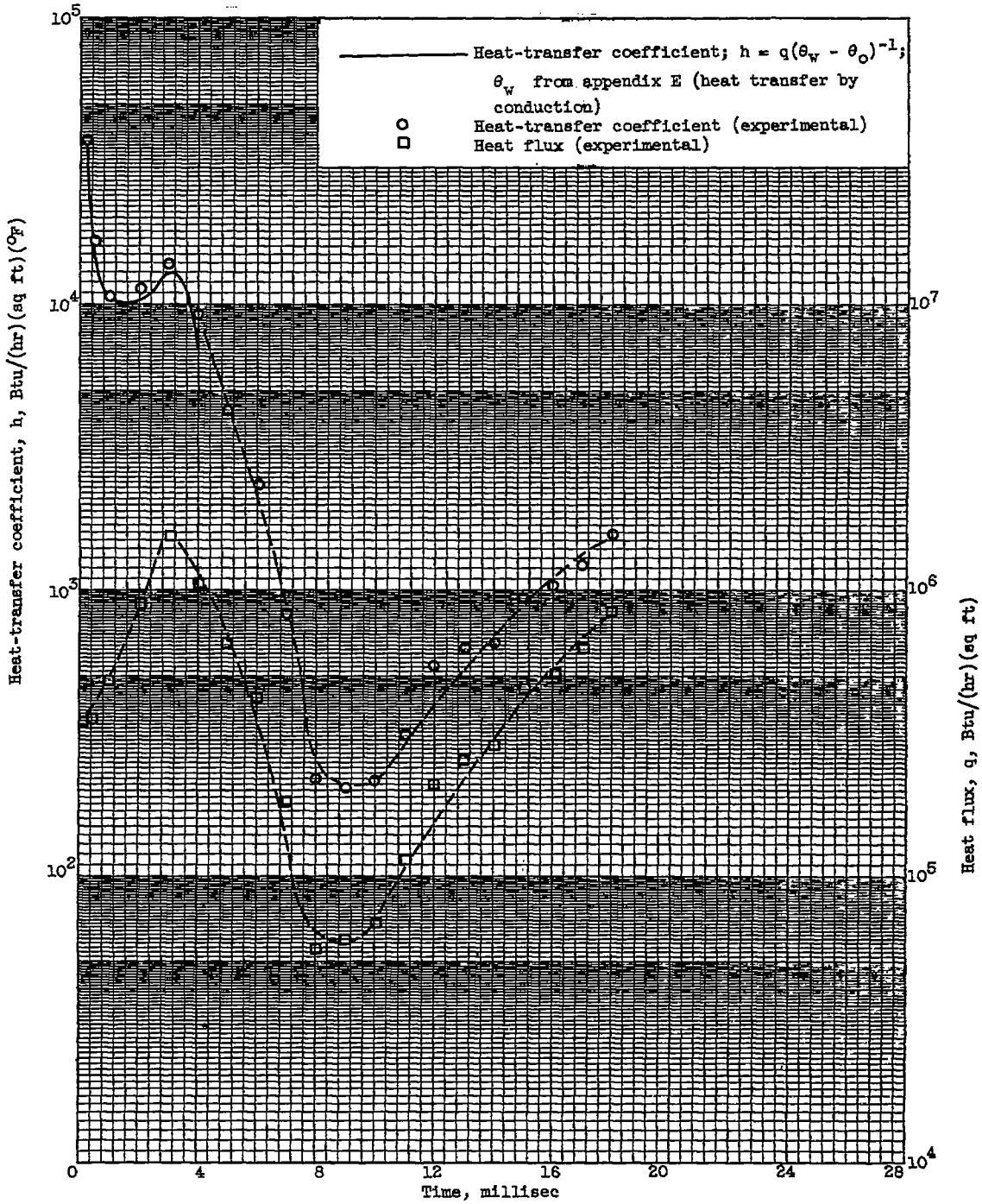

(c) Water temperature, 203° F.

Figure 8. - Concluded. Heat flux and coefficient of heat transfer against time.

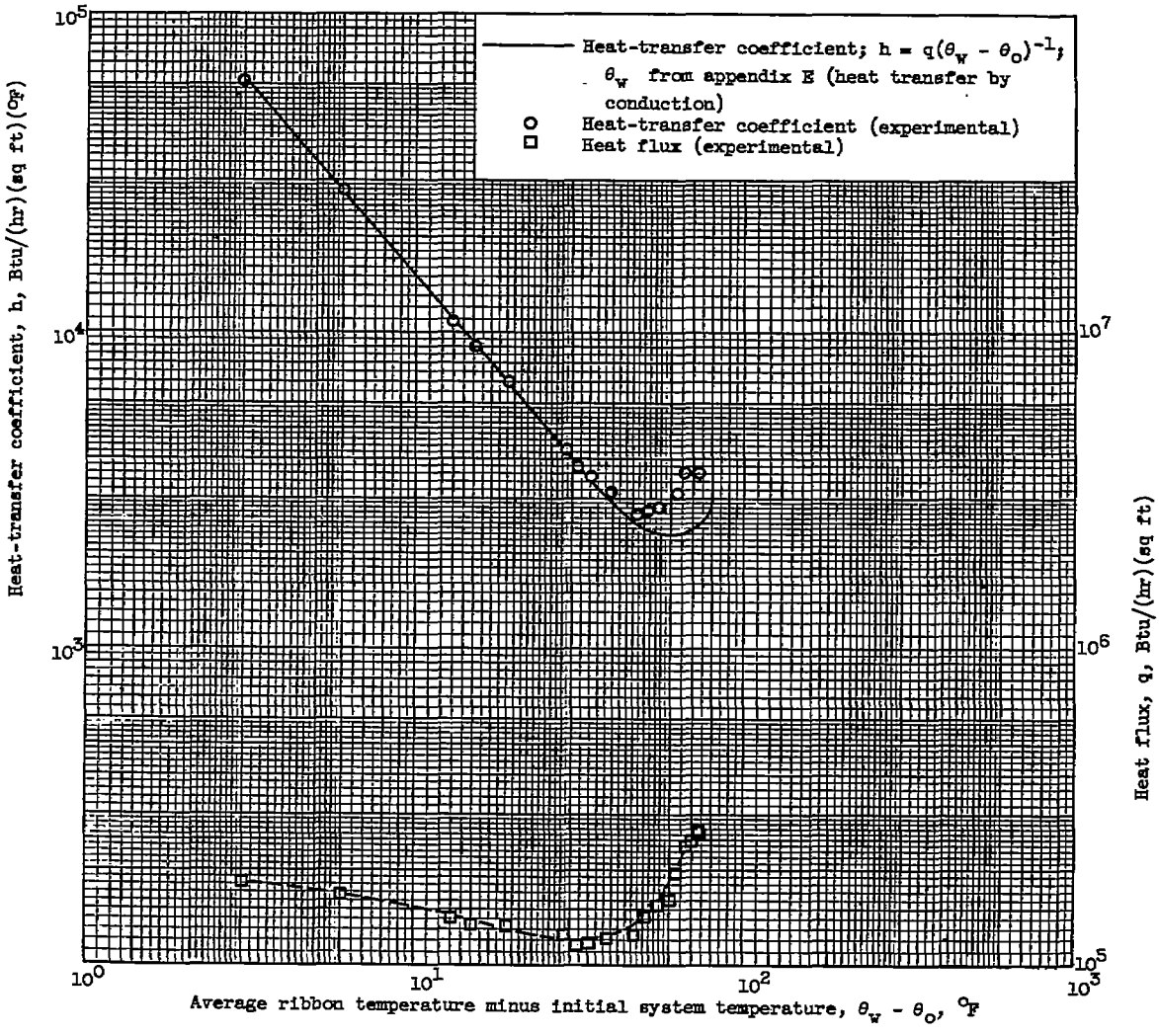

(a) Water temperature, 166° F.

Figure 9. - Heat flux and coefficient of heat transfer against average temperature difference.

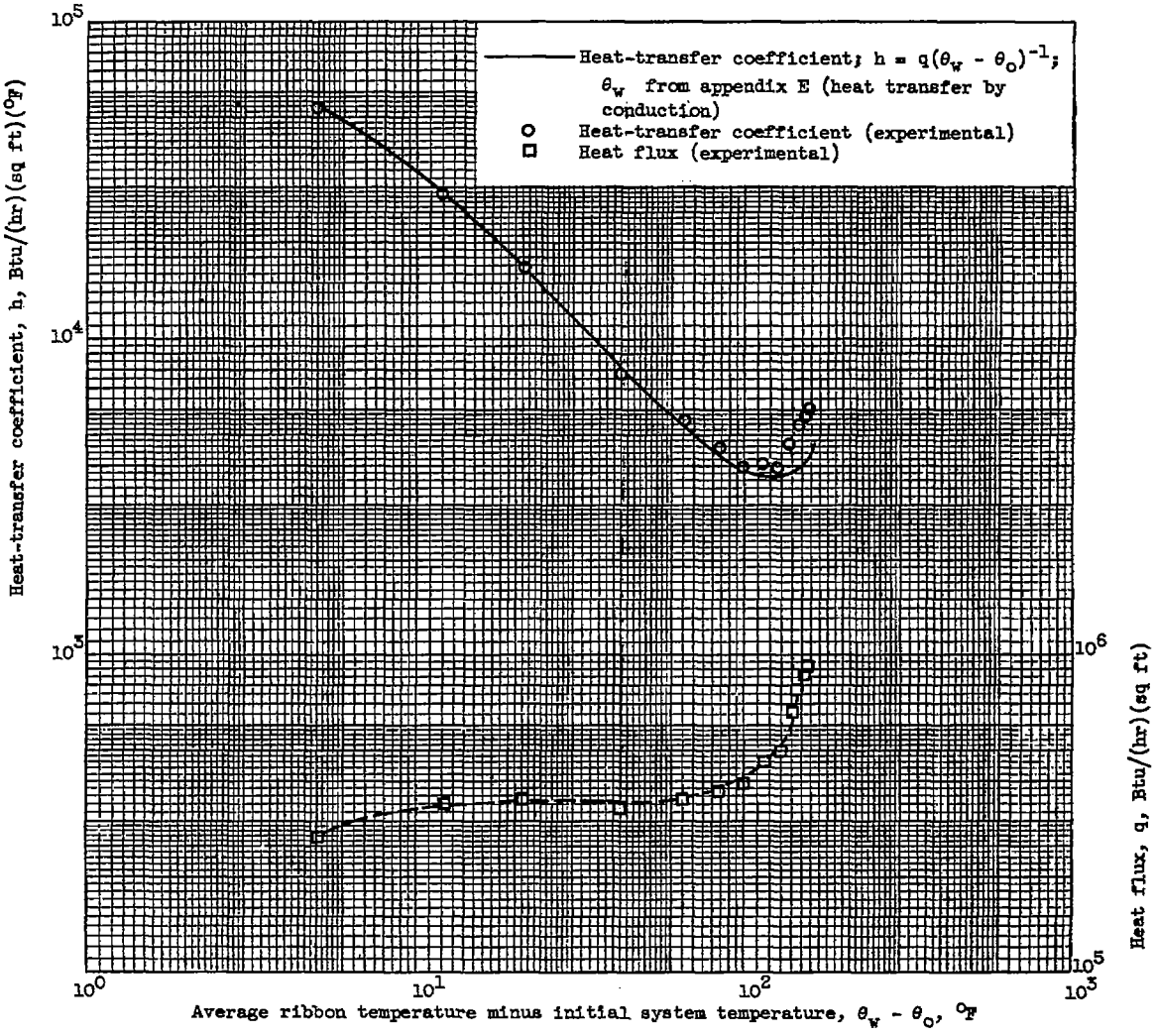

(b) Water temperature, 95° F.

Figure 9. - Continued. Heat flux and coefficient of heat transfer against average temperature difference.

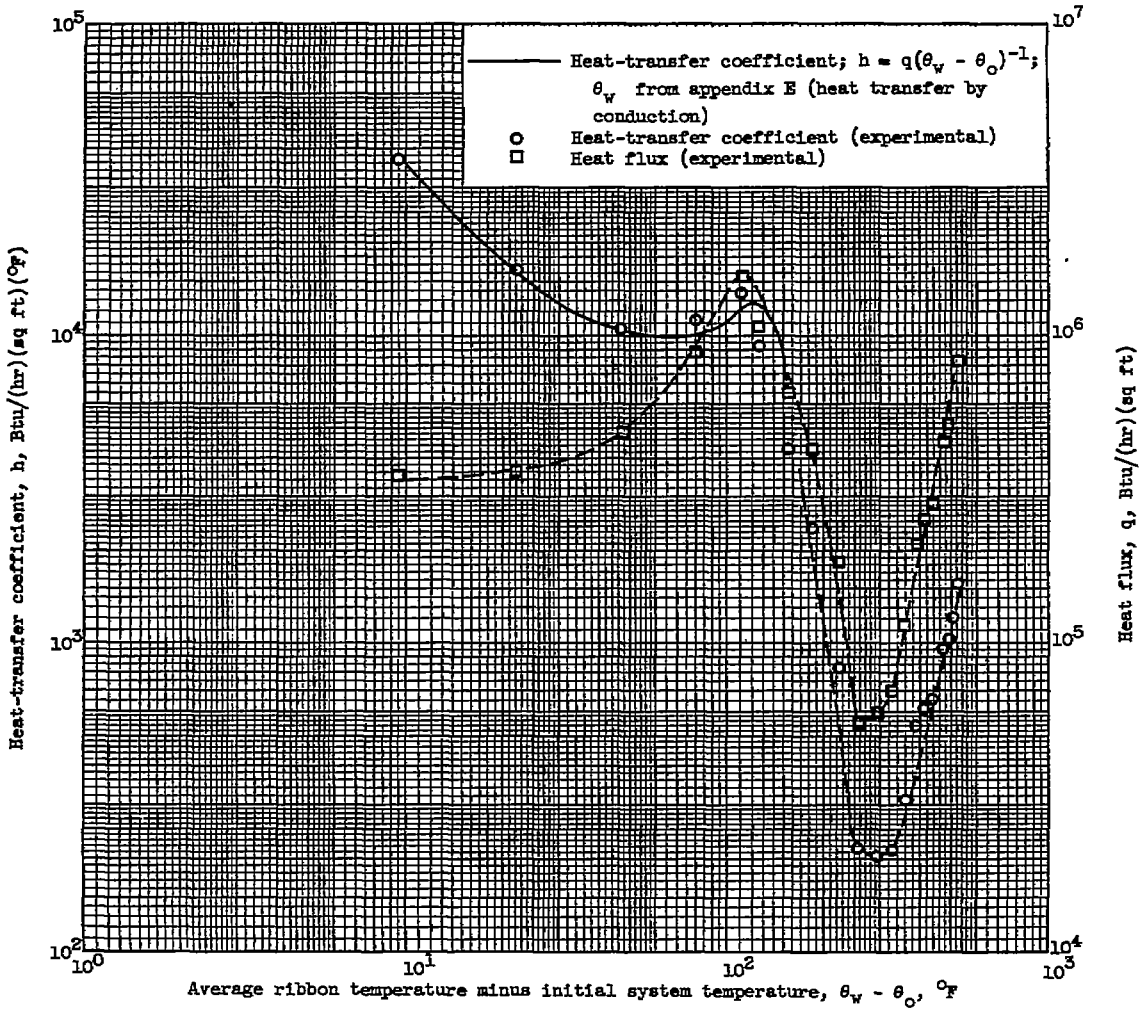

(c) Water temperature, 203° F.

Figure 9. - Concluded. Heat flux and coefficient of heat transfer against average temperature difference.

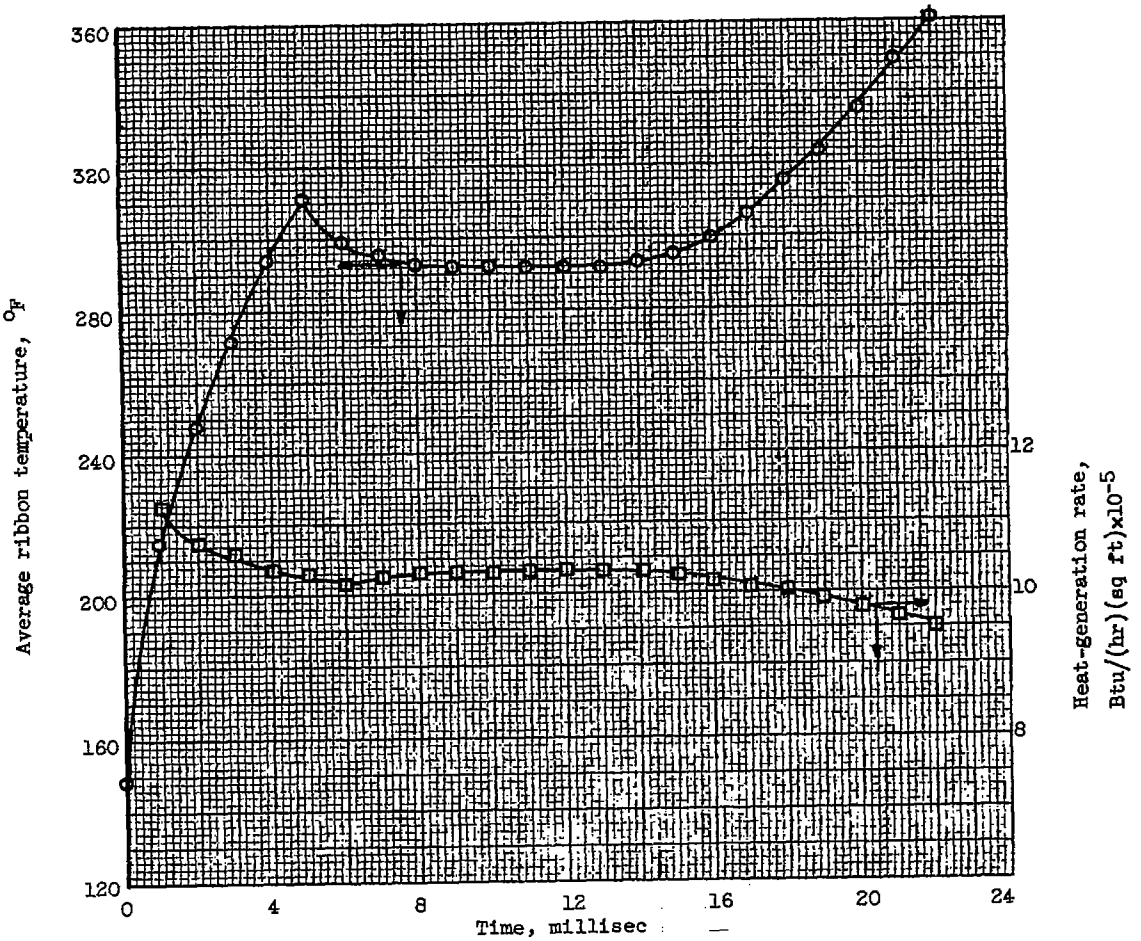

Figure 10. - Temperature - time - heat-generation-rate - time record for nickel ribbon in subcooled water. Initial water temperature, 149° F.

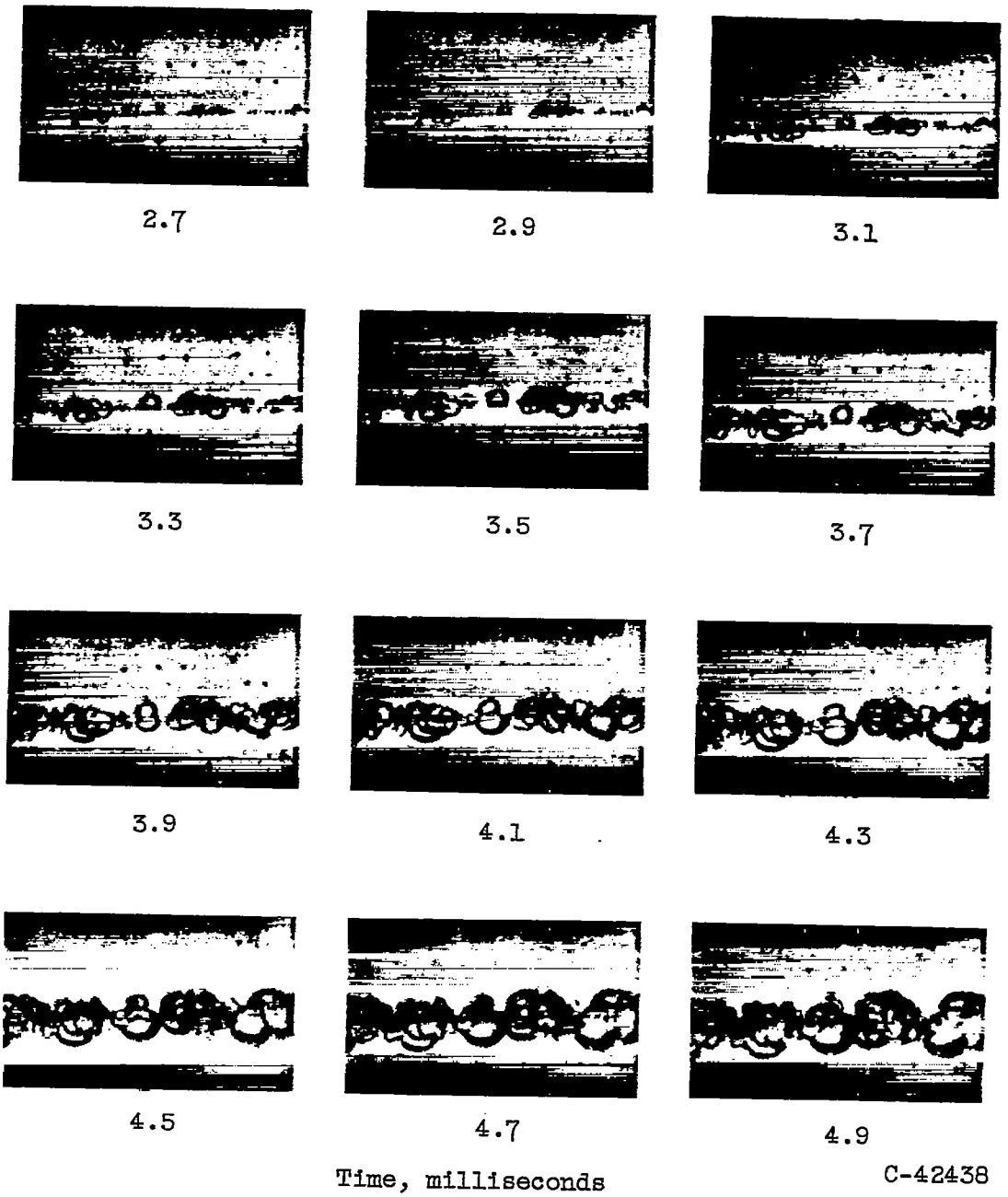

Figure 11. - Transient bubble formation resulting from sudden large power surge. Water temperature, 203° F.

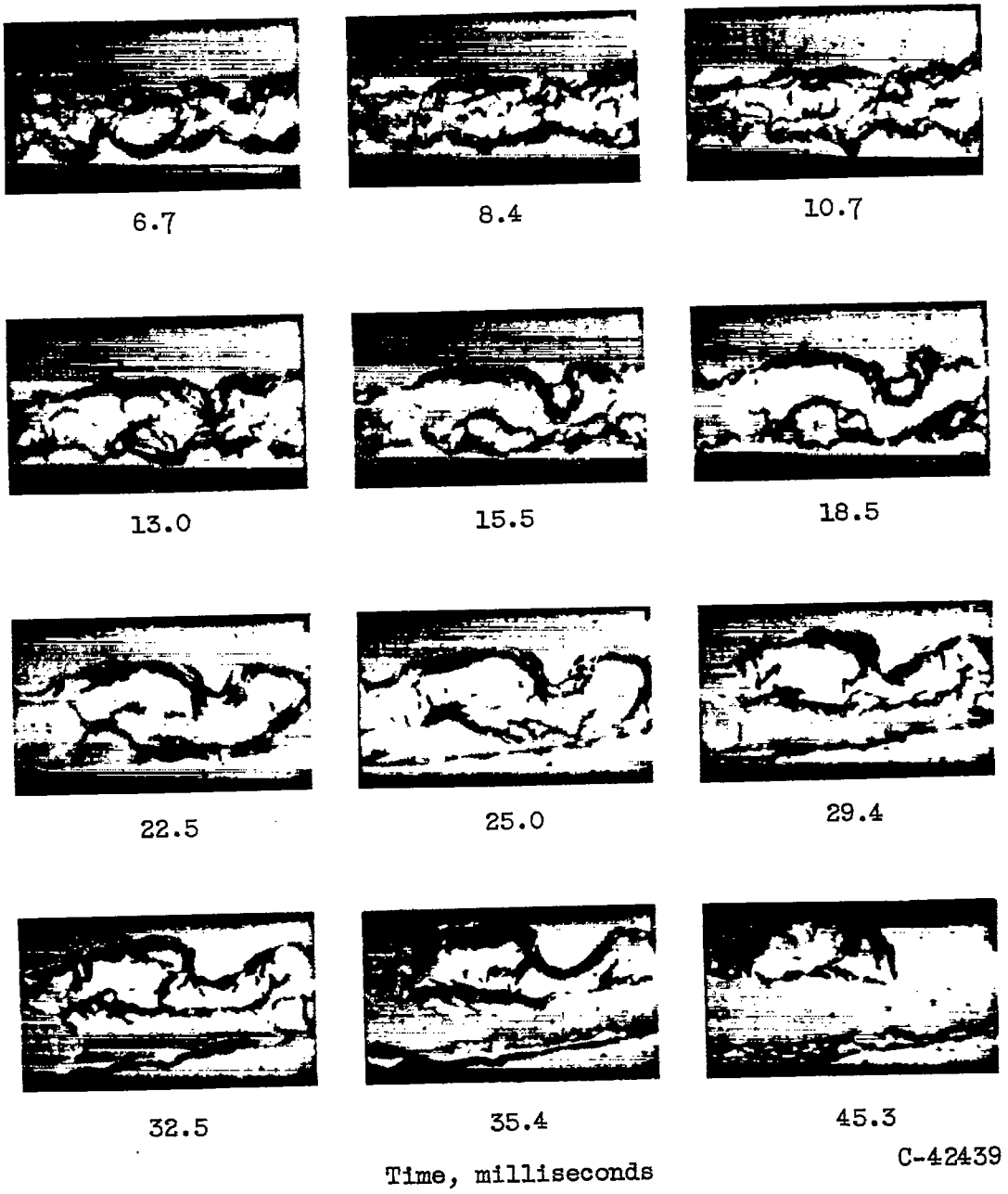

Figure 11. - Concluded. Transient bubble formation resulting from sudden large power surge. Water temperature, 203° F.